
Palaeontology
The Palaeontological Association
www.palass.org

[Palaeontology, Vol. 58, Part 1, 2015, pp. 111–132]

CRYSTALLOGRAPHIC ORIENTATIONS OF STRUCTURAL ELEMENTS IN SKELETONS OF SYRINGOPORICAE (TABULATE CORALS, CARBONIFEROUS): IMPLICATIONS FOR BIOMINERALIZATION PROCESSES IN PALAEOZOIC CORALS

by ISMAEL CORONADO[1], ALBERTO PÉREZ-HUERTA[2] *and* SERGIO RODRÍGUEZ[1,3]

[1]Departamento de Paleontología, Universidad Complutense de Madrid, C/José Antonio Nováis 2, Ciudad Universitaria, E-28040, Madrid, Spain; e-mail: ismael.coronado@geo.ucm.es
[2]Department of Geological Sciences, University of Alabama, Tuscaloosa, AL 35487, USA; e-mail: aphuerta@as.ua.edu
[3]Instituto de Geociencias (IGEO, CSIC-UCM), C/José Antonio Nováis 2, Ciudad Universitaria, E-28040, Madrid, Spain; e-mail: sergrodr@geo.ucm.es

Typescript received 6 May 2014; accepted in revised form 15 July 2014

Abstract: The crystallographic orientation of structural elements in skeletons of representatives of Carboniferous Syringoporicae (Auloporida) has been analysed by scanning electron microscopy (SEM), petrographic microscopy and electron backscatter diffraction (EBSD) on specimens from the Iberian Peninsula. The skeletons of the tabulate corals of the Syringoporicae consist of biogenic calcite crystals, and their microstructure is composed of lamellae, fibres and granules, or of a combination of these. Independent of the microstructure, the *c*-axis is oriented towards the lumen, quasi-perpendicular to the growth direction of the skeleton (perpendicular to the morphological axis lamellae, parallel to fibres). Most phaceloid taxa have a turbostratic distribution, as a biogenic response to prevent the cleavage of crystals. Cerioid and some phaceloid corals, whose microstructure is conditioned by wall elements, do not exhibit turbostratic distribution. Wall elements are determined by the biology of each taxon. Holacanth septal spines are composed of fibres arranged in a cone-shape structure, sometimes clamped to the external part of the corallite and show a complex crystallography. Monacanth septal spines are spindle shaped and composed of bundles of fibres. Tabulae are composed of lamellae. Their development and crystallographic orientation depends on the position of the epithelium in each case. Shared walls are formed by a combination of the walls of two independent corallites with a median lamina, composed of granules; these have a crystallographic orientation between that of the two corallites. The growth of the microstructure is derived by a coordinated stepping mode of growth, similar to other groups of organisms such as molluscs and scleractinians. The nucleation and formation of packages of co-oriented microcrystals suggest a growth mode similar to mineral bridges with a competitive growth mode between each crystal. The growth pattern of corallites suggests that the growth direction is divided into two main components: a horizontal growth direction towards the lumen and a vertical direction towards the top.

Key words: Auloporida, calcite, microstructure, tabulae, septal spines, EBSD.

CALCAREOUS skeletons and shells are important in the development and evolution of numerous organisms because they provide and have provided support and protection throughout the Phanerozoic. Crystalline elements that make up these skeletons are composed of subunits, at micro- and nanoscales, resulting in a hierarchical structure. Each microstructure is formed by one or more multiple elements that keep the proportions, orientations and relationships for optimal biological function. Numerous studies of Recent and fossil corals have demonstrated the value of analysing the microstructure in investigations related to palaeontology, phylogeny, geochemistry and material sciences (Sandberg 1975; Semenoff-Tian-Chansky 1984; Sorauf 1984; Rodríguez 1989; Fedorowski 2001, 2010).

Interest in the microstructure of Palaeozoic corals was initiated in the nineteenth century with classical studies

doi: 10.1111/pala.12127

by Ogilvie (1895) and Struve (1898), and it has remained until the present day. Our knowledge of different microstructures in Palaeozoic corals has improved since the development of ultrathin sections (UTS) by Lafuste (1970). Three principal morphologies were recognized in microstructural elements of Tabulata, Rugosa, and Heterocorallia: fibres, lamellae *sensu lato,* and granules (Lafuste 1970; Semenoff-Tian-Chansky 1974). Different authors have considered microstructure as an important taxonomic character (Lafuste 1970, 1978, 1981, 1983; Lafuste and Plusquellec 1985; Rodríguez 1989; Falces 1997), although comparison with Recent corals has generated an important controversy on this topic. There are three schools of thought regarding the value and interpretation of analysing microstructures in Palaeozoic corals, based on whether or not they are biogenic in nature, as follows: (1) most microstructures have a biogenic origin (Lafuste and Plusquellec 1985; Rodríguez 1989; Falces 1997); (2) only the fibro-normal and trabecular structures have a biogenic origin (Kato 1963; Sorauf 1971, 1978, 1983); and (3) all the recognized structures are products of diagenesis, on the basis that Palaeozoic corals developed an aragonitic mineralogy, as in the Recent Scleractinia (Oekentorp 1984, 2001). Recent studies have demonstrated that the presence of primary skeletal structures can be determined in Cenozoic and Mesozoic coral Scleractinia (Stolarski and Mazur 2005; Stolarski *et al.* 2007). Following this principle, Coronado *et al.* (2013) have shown the original micro- and nanostructures in a study of the skeleton of *Multithecopora hontoriense*, a member of the Syringoporicae from the Carboniferous of Spain.

At the present time, biomineralization studies of Recent and fossil organisms are focused on the crystallographic orientations of the biomineral microstructures because they provide information about the relationships between diverse elements, the processes of growth, and the architectural responses that lead to ecophenotypical variation (Cusack and Williams 2001; Lee *et al.* 2007; Checa *et al.* 2009; Perez-Huerta *et al.* 2011; Cusack *et al.* 2013; Moreno-Azanza *et al.* 2013), as well as to the effects of diagenesis (Perez-Huerta *et al.* 2007, 2012; Cusack *et al.* 2008; Dalbeck *et al.* 2011). For this crystallographic analysis, techniques of X-ray texture and electron backscatter diffraction (EBSD) are commonly used. X-ray texture (XRD-2D) provides information about the crystallographic orientations, mineralogy and crystallinity (Checa and Rodríguez-Navarro 2005; Rodríguez-Navarro 2006; Checa *et al.* 2007). EBSD can also provide additional data about crystal sizes, presence of crystallographic domains and dissolution/recrystallization processes, and it has been applied in mineralogy and palaeontology with significant results (Checa *et al.* 2006; Perez-Huerta and Cusack, 2008; Balthasar *et al.* 2011; Grellet-Tinner *et al.* 2011; Torney *et al.* 2014).

Knowledge of the crystallographic information of skeletal structures in Palaeozoic corals is very limited (Fischer and Lafuste 1972; Coronado *et al.* 2013). The aim of this study was to analyse preferred crystallographic orientations among different microstructural elements in selected taxa, highlighting the processes of growth and the development of wall elements. Four genera of Syringoporicae (Tabulata, Carboniferous), *Multithecopora, Syringopora, Romeripora and Sinopora,* have been studied by high-resolution EBSD, in addition to a comparison with structural data obtained from the analysis of ultrathin sections and scanning electron microscopy (SEM).

SYRINGOPORICAE

The Syringoporicae Fromentel, 1861, comprise taxa that represent marine, colonial sessile organisms that ranged from the Early Ordovician to the Permian and belong to the Order Auloporida (Sokolov, 1947); they are characterized by distinctive morphological features (for more details see Tchudinova 1986; Coronado and Rodríguez 2014). The morphology of the colony depends on the mode of budding and the form and degree of arrangement of the polyps (Tchudinova 1986). The shape of the colony is a manifestation of the biological characters of this group of corals and corresponds also to an ecophenotypical expression. The form of the colony in the superfamily Syringoporicae is fasciculate. The skeletal structure of the colony is variable, most commonly being phaceloid and dendroid, with well-developed connecting structures in the form of tubules or laminae as represented in the main families: Syringoporidae, Multithecoporidae, Tetraporellidae and Sinoporidae (the latter included here in this superfamily because its representatives have closest morphological similarities with Multithecoporidae). The massive fruticose type of corallum, cerioid or pseudocerioid is a variety of the fasciculate type and is less common. It is characterized by a dense, compact arrangement of corallites; the space between corallites is small, or almost nonexistent, as seen in *Roemeripora* and *Neomultithecopora*. Cateniform colonies are even less common; the corallites are arranged in a series of chains, as can be seen in *Enigmalites*, *Neosyringopora* and rarely in *Syringopora*. Fasciculate coralla are characterized by cylindrical corallites with a round cross section, although in some cases they can be cylindroprismatic or pseudopolygonal in cross section. The main characters used in taxonomy have been the distance between corallites, the diameter of the corallite (d), the diameter of the lumen (l), the wall thickness (w) and their corresponding proportions (Fig. 1).

The corallite wall is composed of different layers that form the thecal tissue or microstructure and several morphological wall elements, notably septal elements and tabulae (Fig. 1). Septal elements (septal spines or spinules)

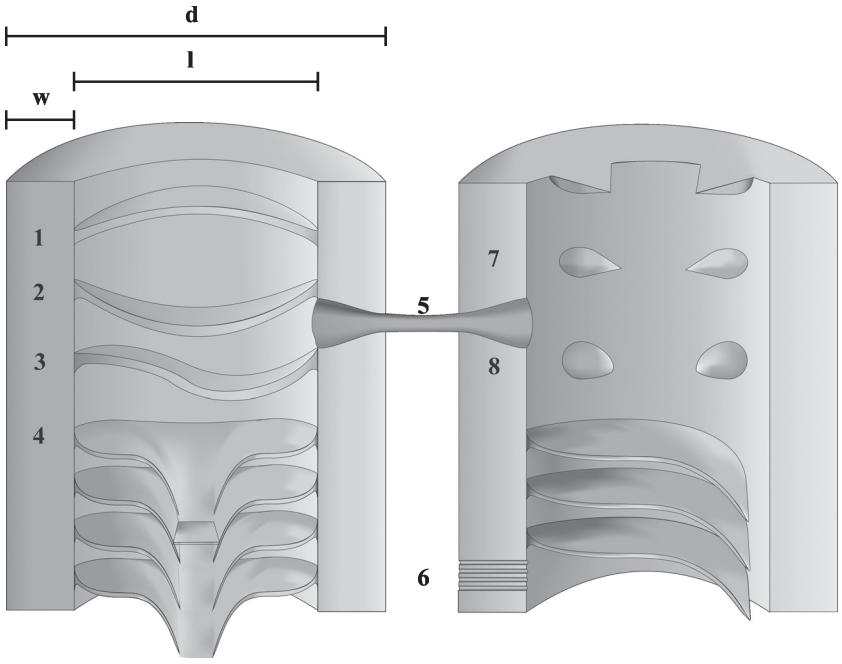

FIG. 1. Main characters used in the taxonomy of the Syringoporicae. *Abbreviations*: d, diameter of corallite; l, lumen diameter; w, wall thickness; 1–4, tabulae forms; 1, convex; 2, concave; 3, irregular; 4, infundibuliform; 5–6, connecting structures; 5, tubuli or stolons; 6, pores; 7–8, septal spines; 7, holacanth spines; 8, monacanth spines.

are very abundant in the Syringoporicae and may have been of great importance in their biological development, although it is unclear what the function of these elements was in the living coral. Septal spines could have served as attachment points to the wall for the polyp and may have aided the retraction of the polyp into the calyx during an increase in water turbidity or energy. Two morphologies of septal spines have been described: subtriangular and acicular (Tchudinova 1986), with the latter projecting further into the lumen. Three types of septal spines have been described on the basis of their microstructure: monacanths, rhabdacanths and holacanths (see Hill 1981 for more details). Tchudinova (1986) described in detail the different types of spinules and their presence in different genera of the Syringoporicae. Tabulae are horizontal elements of the skeleton that extend across the lumen of the corallites. They are attached to the walls of the corallite and serve as a support when the polyp moves upward as the skeletal structure grows. There are several types of tabulae described in Syringoporicae: horizontal, curved (concave, convex, or both) and infundibuliform, with an axial canal (sometimes lateral), incomplete tabulae and variations among them. Other wall elements with importance in the taxonomy of Syringoporicae are columella, dissepiments, connecting elements and diaphragms (Nelson 1962; Tchudinova 1986; Young and Noble 1987).

MATERIAL

Carboniferous tabulate colonies of Syringoporicae were collected from different stratigraphic sections and outcrops from the Iberian Peninsula. Samples correspond to four genera (*Multithecopora*, *Syringopora*, *Roemeripora* and *Sinopora*) and seven different taxa (*Multithecopora* sp. A, *Multithecopora* sp. C, *Multithecopora* sp. D, *Multithecopora hontoriense*, *Roemeripora* sp., *Sinopora* sp. and *Syringopora* sp.). These samples were collected in two different zones of the Iberian Massif in Spain (Ossa-Morena and Cantabrian Zones; Fig. 2). Those from the Ossa-Morena Zone were collected in the Guadiato Area in south-west Spain from two different units (Sierra del Castillo and San Antonio – La Juliana units). The *Multithecopora* sp. A and *Syringopora* sp. samples are from the Antolín section, and the *Multithecopora* sp. C. samples are from the El Collado section, belonging to Sierra del Castillo Unit (Córdoba, Spain), and are of late Visean (early Brigantian) age. The *Roemeripora* sp. samples are from the Fuenteobejuna section and belong to the San Antonio – La Juliana Unit (Córdoba, Spain), which is late Visean (early Brigantian) in age. Those samples collected in the Cantabrian Zone, within the most northern part of the Iberian Massif (Lotze 1945), belong to three different units: Sobia-Bodón, Pisuerga-Carrión and Picos de Europa Units. *Multithecopora* sp. D derived from the Valdeteja – Las Majadas section (Valdeteja Formation, Sobia-Bodón Unit, León, Spain) and are of mid-Bashkirian – early Moscovian (Cheremshankian–Vereian) age. The *Multithecopora hontoriense* samples are from the Playa de la Huelga section (Cuera Limestones Formation, Picos de Europa Unit, Asturias, Spain) which is late Moscovian (Podolskian–Myachkovian) in age. The *Sinopora* sp. samples are from the Celada de Roblecedo section (Vergaño Formation, Pisuerga-Carrión Unit, Palencia,

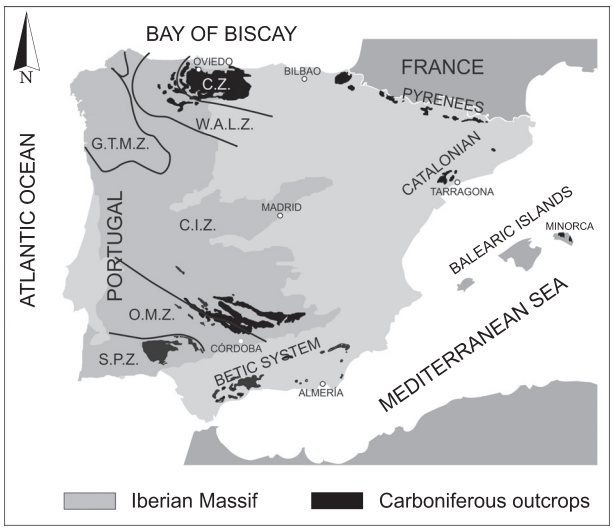

FIG. 2. Distribution of the main Carboniferous outcrops of the Iberian Peninsula. *Abbreviations*: C.Z., Cantabrian Zone; C.I.Z., Central Iberian Zone; G.T.M.Z., Galicia-Tras os Montes Zone; O.M.Z., Ossa–Morena Zone; S.P.Z., South Portuguese Zone; W.A.L.Z., Western Asturian–Leonese Zone. Modified from Colmenero *et al.* (2002).

Spain) which is late Moscovian (Myachkovian) in age. Further details about the localities and palaeobiology of these taxa and samples are given in Coronado and Rodríguez (2014). All samples are reposited in the Palaeontology Department of Complutense University (Madrid, Spain) in the Author Collection Repository. Corresponding catalogue numbers are summarized in Table S1.

METHODS

Complete colonies and fragments were cut longitudinally and transversely, and different slabs were prepared for the application of specific techniques: petrographic microscopy, scanning electron microscopy (SEM) and electron backscatter diffraction (EBSD). A detailed description of these techniques can be found in Appendix S1.

The EBSD data were analysed using the software OIM™ 5.3 from EDAX-TSL. In this study, EBSD data are represented by crystallographic maps and pole figures, which represent the stereographic projection of crystallographic planes in reference to the {0001} calcite plane. MATLAB™ toolbox MTEX (Bachmann *et al.* 2011) was used to plot the ODF (orientation density functions) of the EBSD maps. The GrainsSet is a tool of MTEX that has been chosen to determine grains differentiation, the analysis of misorientation, to plot the orientations of the single crystals and the representation of the pole figures in the planes $\{10\bar{1}0\}, \{01\bar{1}0\}, \{0001\}, \{10\bar{1}4\}$.

The area selected for analysis was adapted to each sample adjusting the map area to the structure or structures studied in each case, including in some cases regions with matrix or sparry cements in the lumen of corals. *Syringopora* sp., *Multithecopora* sp. D and *Multithecopora hontoriense* were chosen to illustrate the relationship between lamellae and fibres, the main crystallographic textures of Syringoporicae, whereas *Roemeripora* sp. was selected to study the crystallographic variation in corals with a cerioid growth form. In addition, *Multithecopora* sp. A and *Multithecopora* sp. C were chosen to study the crystallographic distribution and relationships between different microstructural elements in different septal spines. Finally, *Sinopora* sp. was selected to study the crystallographic properties of the tabulae and their relations with the other microstructural elements.

RESULTS

Microstructure in tabulate corals

Three principal kinds of calcite crystals are recognized in the studied taxa: lamellae, fibres and granules. Regardless of the morphology of the crystals, all the elements have common crystallographic characteristics. Pole figures of the $\{10\bar{1}0\}$ planes show a strong maximum separated by ~60° in relation to the trigonal symmetry of calcite (Fig. 3). The stereographic projection of poles, with reference to $\{10\bar{1}4\}$, shows three pole maxima in each crystal, each pair separated by ~75°, which corresponds to the angular distance between the faces $(104), (0\bar{1}4)$ and $(\bar{1}14)$. The angular distance between the faces (001) and (104) is ~44° (Fig. 3). For simplification and better visualization, these characteristics are based on a rhombohedral morphology of the calcite crystal lattice for each microstructural element, although the overall configuration is hexagonal. The *c*-axis orientation varies with respect to the morphological axis between each crystallographic element. Details of the dimensions of the microstructural elements of the samples studied are summarized in Table 1.

Lamellae and microlamellae (*sensu* Rodríguez 1989) are flat crystals (like scales or shields, Fig. 3), slightly curved and in section show indentations to their edges and flake forms. These structures have a great lateral development in two dimensions; their length varies from 5 to 37 μm, and their width fluctuates from 2 to 6 μm depending on the taxon (Table 1). Crystals are imbricated in both the vertical and horizontal directions, and their disposition is always with the morphological axis in the growth direction. The convex part of the lamellae is always oriented to the external part. The *c*-axis of these elements is located quasi-perpendicular to the morphological axis.

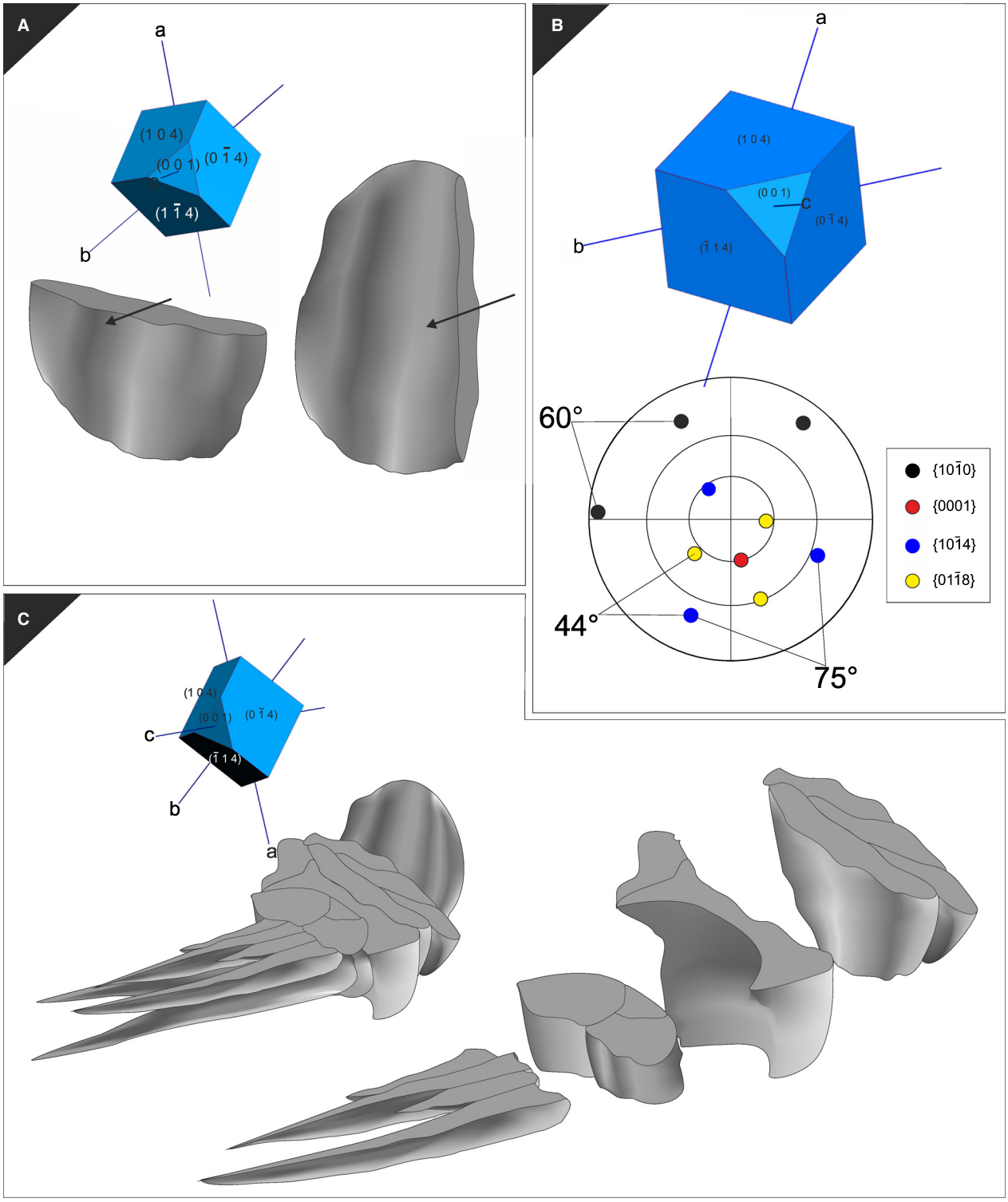

FIG. 3. A, interpretations of the crystallography of a lamella showing transverse and longitudinal sections. Rhombohedron sketches produced using WinXMorph (Kaminsky, 2007) from main reflections of a single lamella and fibre. B, main reflections of lamellae and their distribution in the theoretical rhombohedra. C, transition from lamellae to fibres and the theoretical rhombohedra pointing to the *c*-axis direction.

TABLE 1. Dimensions of microstructural elements of Syringoporicae from this study.

	Microstructure		Dimensions L (μm)		Dimensions F (μm)		Dimensions G (μm)	
Taxa	L, F, G	Observations	Length	Width	Length	Width	Length	Width
Multithecopora sp. A	F–L–F	Thin inner fibrous domains	$\bar{x}$ = 15 (9–22)	$\bar{x}$ = 3 (2–4)	$\bar{x}$ = 20 (16–32)	$\bar{x}$ = 6 (3–8)	–	–
Multithecopora sp. C	L–F	Lamellar and inner fibrous domains	$\bar{x}$ = 20 (9–33)	$\bar{x}$ = 3 (2–6)	$\bar{x}$ = 21 (13–39)	$\bar{x}$ = 4 (1–6)	–	–
Multithecopora sp. D	L–F	Thick inner fibrous domain	$\bar{x}$ = 21 (13–37)	$\bar{x}$ = 4 (2–6)	$\bar{x}$ = 29 (17–42)	$\bar{x}$ = 4 (3–6)	–	–
Multithecopora hontoriense	F–L–F–L–F	Middle fibrous domain sometimes absent	$\bar{x}$ = 22 (5–35)	$\bar{x}$ = 4 (2–5)	$\bar{x}$ = 21(15–33)	$\bar{x}$ = 4 (2–5)	–	–
Sinopora sp.	F–L–F	Thin inner fibrous domain	$\bar{x}$ = 16 (5–30)	$\bar{x}$ = 3 (2–4)	$\bar{x}$ = 19 (12–30)	$\bar{x}$ = 3 (2–5)	–	–
Roemeripora sp.	G–L–F	External granular domain	$\bar{x}$ = 12 (8–15)	$\bar{x}$ = 3 (2–4)	$\bar{x}$ = 21 (10–38)	$\bar{x}$ = 2 (1–3)	$\bar{x}$ = 6 (3–9)	$\bar{x}$ = 4 (2–6)
Syringopora sp.	F–L	External fibrous domain	$\bar{x}$ = 20 (9–27)	$\bar{x}$ = 3 (2–4)	$\bar{x}$ = 29 (50–17)	$\bar{x}$ = 4 (3–6)	–	–

L, lamellae; F, fibres; G, granules.

Fibres are also common crystallographic elements that form the microstructure of tabulate corals. They are elongate crystals with irregular morphology, indentations to their edges and an apex or tip at the end of the fibres and, in some cases, also at the base. In some cases, they are barrel-shaped or tabular, depending on their situation in the skeleton, but they are never needle-shaped fibres, as in scleractinian corals. Their length varies from 10 to 42 μm, and their width fluctuates from 1 to 8 μm depending on the taxon (Table 1). The morphological axis is consistently oriented towards the lumen, perpendicular to the direction of growth, and the *c*-axis is parallel to the morphological axis.

Granules are visible only in *Roemeripora* sp., the only cerioid form studied, and are located in the median lamina (dark lamina) between two corallites. The granules are equidimensional crystals, with indentations to their edges, flake morphologies and irregular distribution. They form the median lamina, but its dark appearance is related to the distribution and morphology of granules and their degree of imbrication. Granules have irregular sizes with lengths from 3 to 9 μm, and their width fluctuates from 2 to 6 μm.

An inherent characteristic of Palaeozoic corals is the gradual transition between crystallographic elements (e.g. lamellae to fibres). This gradual transition has previously been described by numerous authors (Semenoff-Tian-Chansky 1974; Lafuste 1978, 1983; Rodríguez 1989, Falces and Rodríguez 1999). These elements change their morphology gradually (Figs 3, 4), independently of taxon and order, as can be seen in the schematic representation of microstructures in Figure 3; the EBSD data show that they maintain the crystallographic orientation in the gradual transition. Sometimes, a branch-off in the transit point where two or more fibres are initiated can be seen, but the preferred crystallographic orientation remains constant (Fig. 4).

A single crystallographic texture

All the Syringoporicae studied in this work present a crystallographic texture with common features. All the layers of the microstructure of each taxon show a preferred orientation of the crystals around the *c*-axis, which is always quasi-perpendicular to the growth direction of the

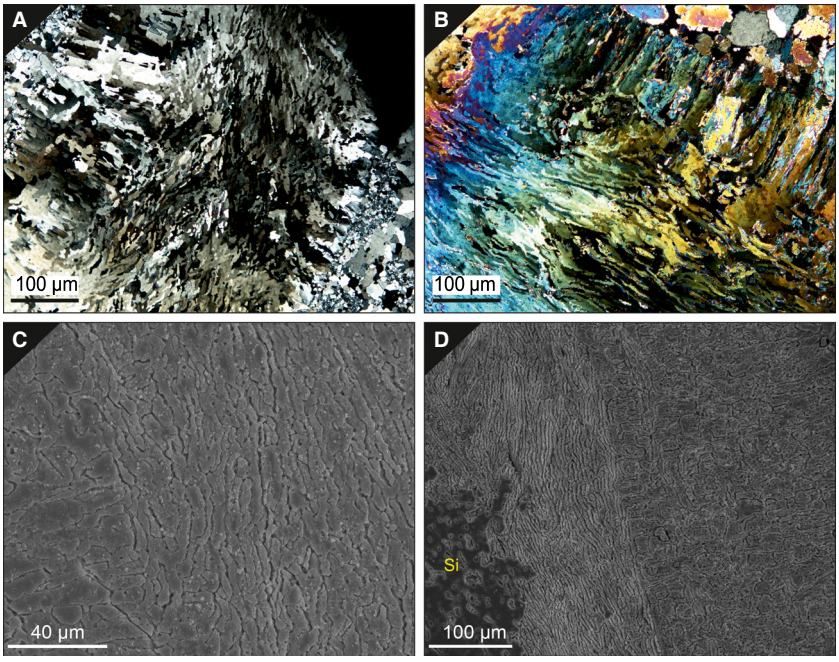

FIG. 4. A–B, petrographic images of ultrathin sections of two representatives of the Syringoporicae where the gradual transition from lamellae to fibres is shown; A, *Sinopora* sp.; B, *Syringopora* sp. C–D, SEM images showing the gradual transition from lamellae to fibres; C, *Multithecopora hontoriense*; D, *Multithecopora* sp., note the preservation of lamellae between and around the silicification process (Si) of the external edge of the corallite.

skeleton, radial to the cylindrical section of the corallite (Fig. 3). Phaceloid taxa (*Syringopora* sp., *Multithecopora* sp. D, *Multithecopora hontoriense* and *Sinopora* sp.) have a rotation around the *c*-axis of the crystals, as can be seen in the pole figures of the plane $\{10\bar{1}4\}$ (Fig. 5), and this distribution has been defined as turbostratic development (Checa *et al.* 2007). In the pole figure representing the $\{10\bar{1}0\}$ and $\{01\bar{1}0\}$ planes, the colours show the orientations of crystals with similar *c*-axis orientation (Fig. 5B). The variation of each colour is at ~15° around a curved line (broad distribution, ~30°). This special development can be explained by the rotation of the calcite crystals along the *a*- and *b*-axes (~15°), maintaining the fixed *c*-axis. Figure 5C shows the ODF representation of the orientation of the phaceloid coral *Sinopora* sp. and *Multithecopora hontoriense* and the rotation of the pole maxima of the *a*- and *b*-axes around the *c*-axis, showing a circular pattern with three pole maxima in each plane belonging to (104) faces.

In contrast, in the cerioid taxon *Roemeripora*, turbostratic development is not present on the plane $\{10\bar{1}4\}$ or other tautozonal planes. Pole figures of the plane $\{10\bar{1}4\}$ indicate that the calcite crystals are biaxially aligned (Fig. 5C). *Roemeripora* shows a polygonal development with a pseudohexagonal morphology (Fig. 5A). Each wall in *Roemeripora* is shared with another polyp. These subwalls (six in total) show different crystallographic orientations, as is visible in the ultrathin sections and EBSD maps (Figs 5, 6). The rotation of each polygonal wall of *Roemeripora* is 60°; consequently, the crystals of the microstructure turn each 30°. Figure 5C shows that clusters of crystals of *Roemeripora* each turn ~30° in the plane $\{10\bar{1}0\}$ due to this arrangement. On the other hand, *Multithecopora* sp. A and *Multithecopora* sp. C show a partial loss of their turbostratic distribution in the lamellae zones between two areas very close to the septal spines (Fig. 5C). The lamellae are strongly oriented, adapting to the morphology of the septal spine that does not show this kind of distribution. In the EBSD crystallographic map, the lamellae can be observed as a wavy distribution between the septal spines (Fig. 7G–H).

Misorientation can be used to describe the relative orientation between two neighbouring grains (Frank and Medalist 1988) and is measured as the number of degrees required to bring these two grains into crystallographic alignment on a common axis (Frank and Medalist 1988; Rajan 2000; Dalbeck and Cusack 2006). Misorientation in these corals has been analysed with the MTEX tool, which measures the different crystallographic orientation between two grains (crystals) which are in contact. In the first place, it was necessary to establish the grains in the EBSD crystallographic map, taking a threshold of 2° to reduce the noise within each crystal. Subsequently, misorientation histograms were generated to indicate the main order of misorientation that each sample has (Fig. S1). Several recurrent correlated and uncorrelated misorientations are present in the samples of representatives of the Syringoporicae (Fig. S1), and their variations depend on each section of the coral. The most common misorientation is less than 5°, with a mode of ~2.5°, in both transverse and longitudinal sections. Where the sections are cut obliquely to the transverse section, bar

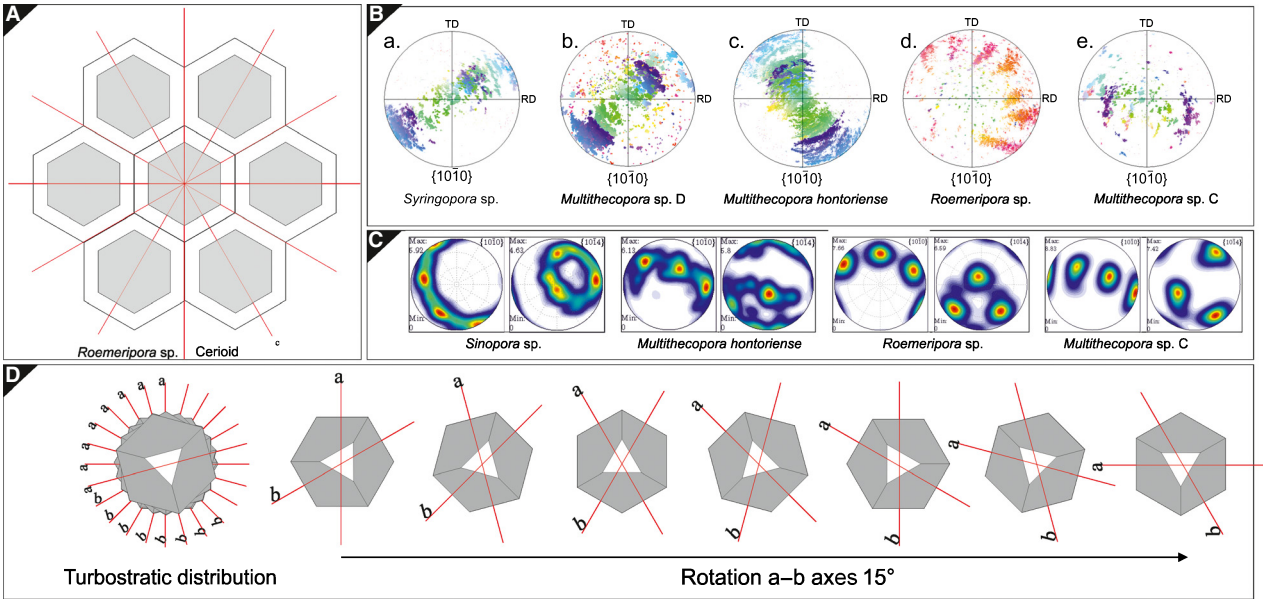

FIG. 5. A, schematic distribution of cerioid growth of *Roemeripora* sp. Each red line corresponds to a turn of 60°. B, pole figures of different taxa (in normal direction view (ND) to the sample surface in a three axes reference system with indication of the reference (RD) and transverse (TD) directions) indicating crystallographic orientation of calcite crystals with reference to the *a*-axis. a–c, taxa that have a turbostratic distribution of their crystals; d–e, taxa that do not have a turbostratic distribution. C, ODF pole figures of different taxa with or without turbostratic distribution. D, schematic interpretation of turning *a*- and *b*-axes by 15° around *c*-axis in a turbostratic distribution.

diagrams exhibit a flat distribution of correlated and uncorrelated misorientation, the second most common being ~15°. The next maxima of misorientation vary for each taxon, the most common being ~24°, 33°, 40° and 60°. Uncorrelated misorientation patterns most similar between longitudinal sections show a normal distribution with a maximum around 50°–55°. *Roemeripora* exhibits a bimodal distribution with two maxima, one at 15° and the other at 65°, and the correlated misorientation is normal, with a maximum at 5°.

Structure of the wall elements (septal spines, tabulae and shared walls)

Crystallographic orientation and properties of different wall elements were analysed using EBSD. Different taxonomic characters of the seven taxa studied, including the wall elements, are summarized in Table S1.

Septal spines. The septal spines selected are acicular holacanths present in *Multithecopora* sp. A (Fig. 7) and subtriangular monacanths in *Multithecopora* sp. C (Fig. 8). The microstructure of holacanth spines is a trabecular structure embedded in lamellar sclerenchyma. The trabecular microstructure was described by Kato (1963) in Rugosa septa, as divergent fibres that are bundled in a series of cone-like invaginations. Holacanth septal spines in *Multithecopora* sp. A are formed by irregular fibres, divergent or lightly tilted, with respect to the axial plane of the spine (morphological axis), that maintain the same or similar orientation and form a cone-like structure. These cones are stacked keeping the morphological axis in the centre of spine (Fig. 7F, I). Three areas in the septal spine can be recognized by the crystallographic orientation of their crystals: origin of the spine, core of the spine and cone-like structures. The origin of the spine is the first cone bundle, which is directly attached to the lamellar sclerenchyma. In a few cases, holacanth spines, projecting through the coral wall to the external edge, develop an 'egg-box-shaped' structure (Fig. 9E), during the adaptation of lamellae to the spine, as observed in tangential sections. The crystals in the core of spine have the *c*-axis oriented parallel to the morphological axis of the spine, and coupled *a*- and *b*-axes are perpendicular. In contrast, in the origin of the spine, the *c*-axis is tilted at 40° with respect to the core of spine, and coupled *a*- and *b*-axes are orientated almost perpendicular, in a more broad distribution, due to the cone-like distribution of the crystals. The tilted variations in *c*-axis have been measured in different crystals belonging to the cone-like structures that form the septal spine. The maximum tilt recorded is ~100° between the crystals, with a variation of the *c*-axis orientations of ~5°, 18°, 25–30°, 40° and 55°,

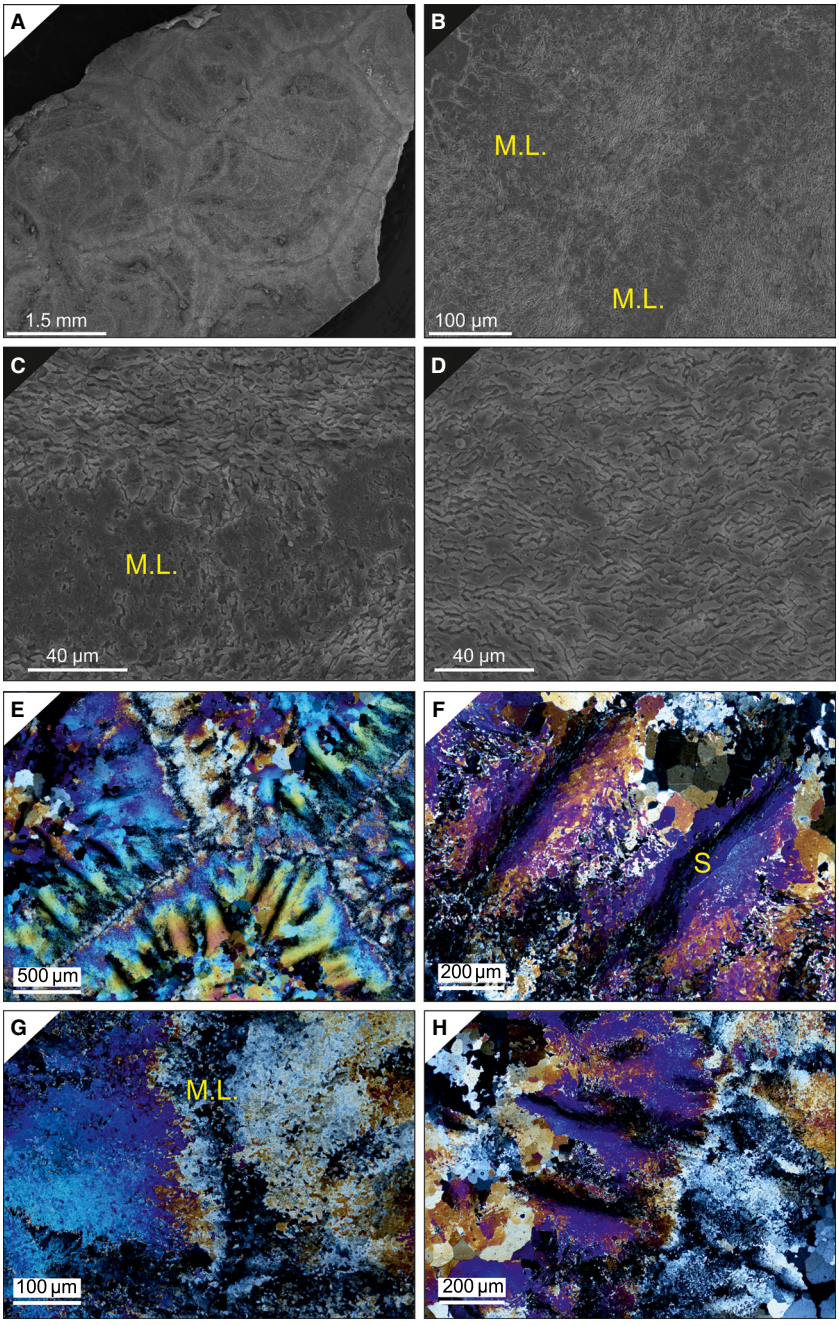

FIG. 6. A–D, SEM images of *Roemeripora* sp.; A, general view of cerioid growth of colony; B, contact point between three corallites, M.L. is the median lamina; C, detail of median lamina (M.L.) between two corallites; note the transition between the lamellae and granules; D, detail of the lamellae that form the coral wall. E–H, petrographic images of ultrathin sections of *Roemeripora* sp.; E, note the median lamina and the subpolygonal morphology of corallites; F, detail of holacanth septal spines (S) of *Roemeripora* sp., note the wavy distribution of lamellae between spines; G, detail of contact between two corallites, note the difference between interference colours, indicating different orientation of the *c*-axes; H, contact between two corallites, note the alignment of septal spines in both corals.

similar to the misorientations recorded in the wall. Lamellae surrounding septal spines are rotated and adapt their morphology to the spines, covering the structure with lamellae (Fig. 7G–I). The *c*-axis is orientated perpendicular to the morphological axis of the spine. The septal spines are very close to each other in *Multithecopora* sp. A, so the lamellae have an undulating appearance.

Holacanth spines can be observed in ultrathin sections of other taxa such as *Roemeripora* sp. (Fig. 6E–H), *Syringopora* sp. (Fig. 9E–F), and in a few examples of *Sinopora* sp. Interference colours in ultrathin sections of *Syringopora* sp. and *Roemeripora* sp. show that crystals of the cores of septal spines are oriented similarly to those observed in *Multithecopora* sp. A by EBSD, except that in *Syringopora* sp. the spines are not too close together and the wall lamellae exhibit an irregular turbostratic distribution (Fig. 10). In *Roemeripora* sp., the spines are very close and the turbostratic distribution is not present (Fig. 5).

Subtriangular monacanth septal spines, not strongly developed, appear in *Multithecopora* sp. C (Fig. 8) and show a more simple structure than that of holacanth

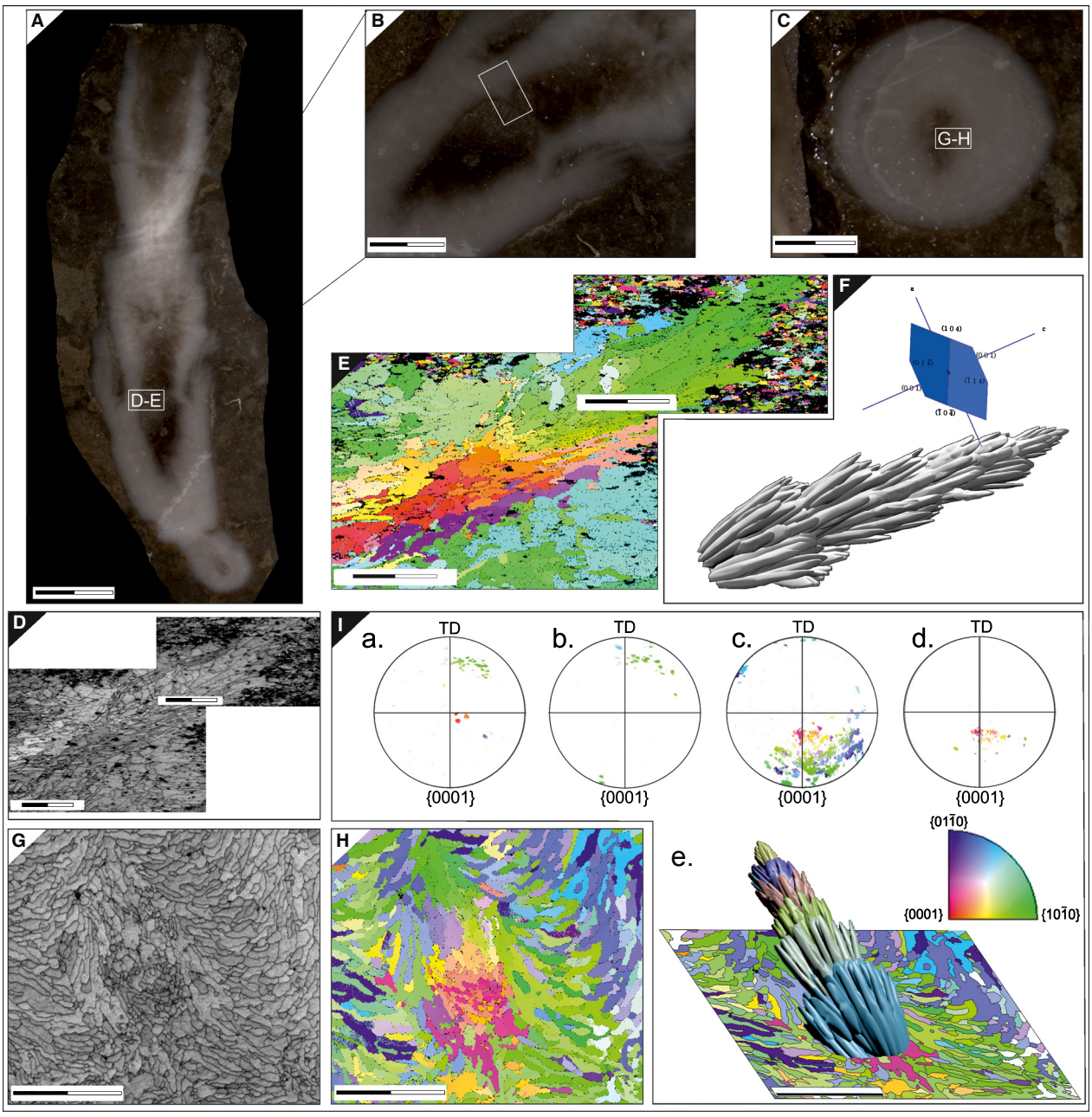

FIG. 7. A–C, skeleton of *Multithecopora* sp. A and location of the EBSD maps (white rectangles); A, longitudinal section; B, detail of holacanth septal spine; C, transverse section. D–E, EBSD images showing crystallography of holacanth septal spine shown in A and B; D, index intensity map, showing the structure of the spine formed by fibres and the surrounding micrite; E, crystallographic orientation map, showing the main crystallographic orientations in the fibrous cone-like regions of the septal spine; note the colours of different cone-like structures that form the spine. F, 3D interpretative sketch of a septal spine and the theoretical rhombohedron pointing to its growth direction. G–H, EBSD images showing crystallography of core septal spine and surrounding lamellar domain; G, index intensity map, showing a detail of the structure of the core of a septal spine, the morphology of the crystals and their crystallographic correlation; H, crystallographic orientation map; note the wavy surrounding lamellae and the different orientation of the core of the septal spine. I, pole figures (in normal direction view (ND) to the sample surface in a three axes reference system) indicating the crystallographic orientation of calcite crystals with reference to the *c*-axes; and crystallographic key indicating colour coding of crystallographic axes; a–b, septal spine shown in D–E, red colour (bottom left of key) specifies the core and green (bottom right) the fibres of the cone-like tip; c–d, orientation distribution of septal spine core shown in G–H; d, detail of core of spine; e, 3D interpretative sketch of a septal spine over an orientation image showing the distribution of cone-like and wavy lamellae adapting to the development of spine. Scale bars represent 2 mm (A); 1 mm (B–C); 50 μm (D–E); and 100 μm (G–H).

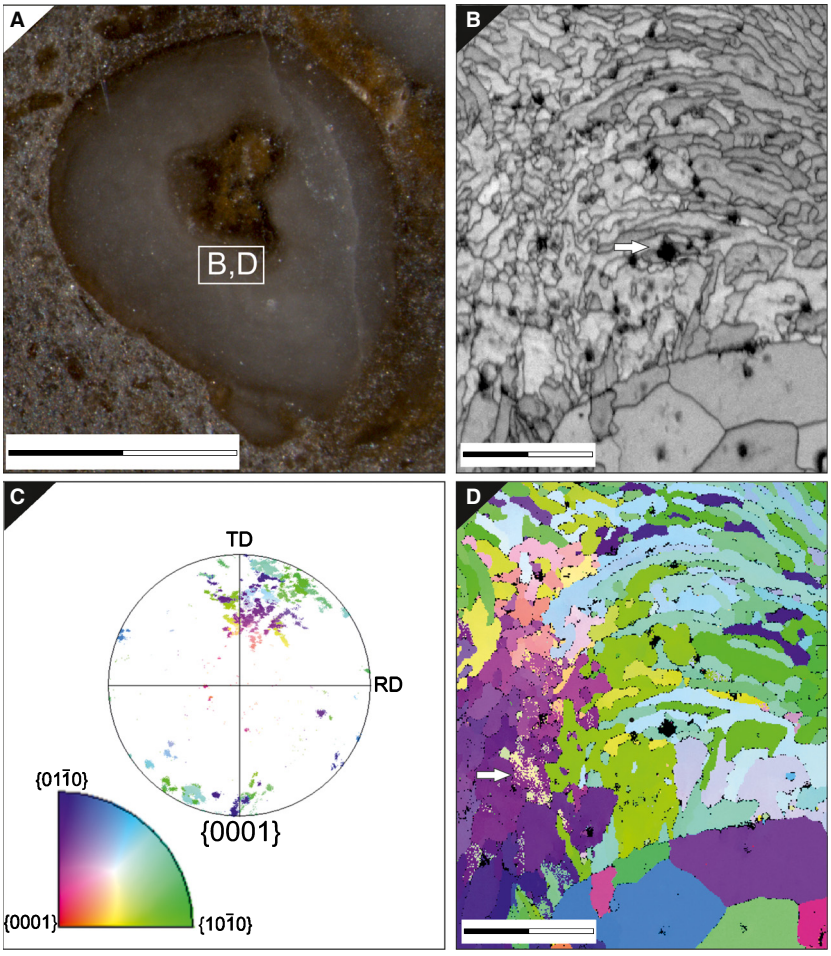

FIG. 8. *Multithecopora* sp. C. A, transverse section of the skeleton and location of the EBSD maps (white rectangle). B, D, EBSD images showing crystallography of a monacanth septal spine; B, index intensity map, showing the structure of the spine formed by fibres and the surrounding sparry calcite; note the black points of dissolution, a product of diagenesis; D, crystallographic orientation map, showing the main crystallographic orientations in the development of a septal spine; note the different colours of fibres that form the spine and the gradual transition between the lamellae of wall and the fibres of the spine, and the transition between the fibres of the inner domain and the fibres of septal spine. White arrow points to some crystals that show an alteration pattern, with different orientation. C, pole figure (in normal direction view (ND) to the sample surface in a three axes reference system with indication of the reference (RD) and transverse (TD) directions) indicating the crystallographic orientation of calcite crystals with reference to the *c*-axis; and a crystallographic key indicating colour coding of crystallographic axes; note that the orientation of the septal spine is similar to the orientation of the lamellae of wall, and the points with random orientations correspond to sparry calcite crystals. Scale bars represent 1 mm (A) and 50 μm (B, D).

spines. The septal spine is a spindle-shaped structure composed of bundles of fibres that diverge slightly. In the case of *Multithecopora* sp. C, the inner fibrous domain surrounds the spine; deeper in the wall, the spines are surrounded by lamellae (Fig. 8B). The origin of the spine is composed of fibres that are produced initially as a package of lamellae, which was folded in an inflexion zone and turned to the direction of the fibres (Fig. 8B, D). This feature is reminiscent of that of holacanth spines, but with a short development not leading to the formation of cone-like structures. Although the core of the septal spine has a preferred orientation, parallel to the morphological axis of the spine, lateral crystals are open, surrounding the core because these fibres belong to the inner fibre domain. In all cases, the *c*-axis is parallel to the morphological axis of the spine. The misorientation of crystals inside the spine is mainly less than 30°, being ~5° in the first order, and ~15°, 20° and 25° in subsequent orders. In the case of *Multithecopora* sp. C, the septal spines are less common and they do not have a turbostratic distribution in the lamellae of the wall (Fig. 5C).

Tabulae. Tabulae are the other main wall element in Syringoporicae. A longitudinal section of *Sinopora* sp. was analysed at the peripheral origin of a tabula by EBSD.

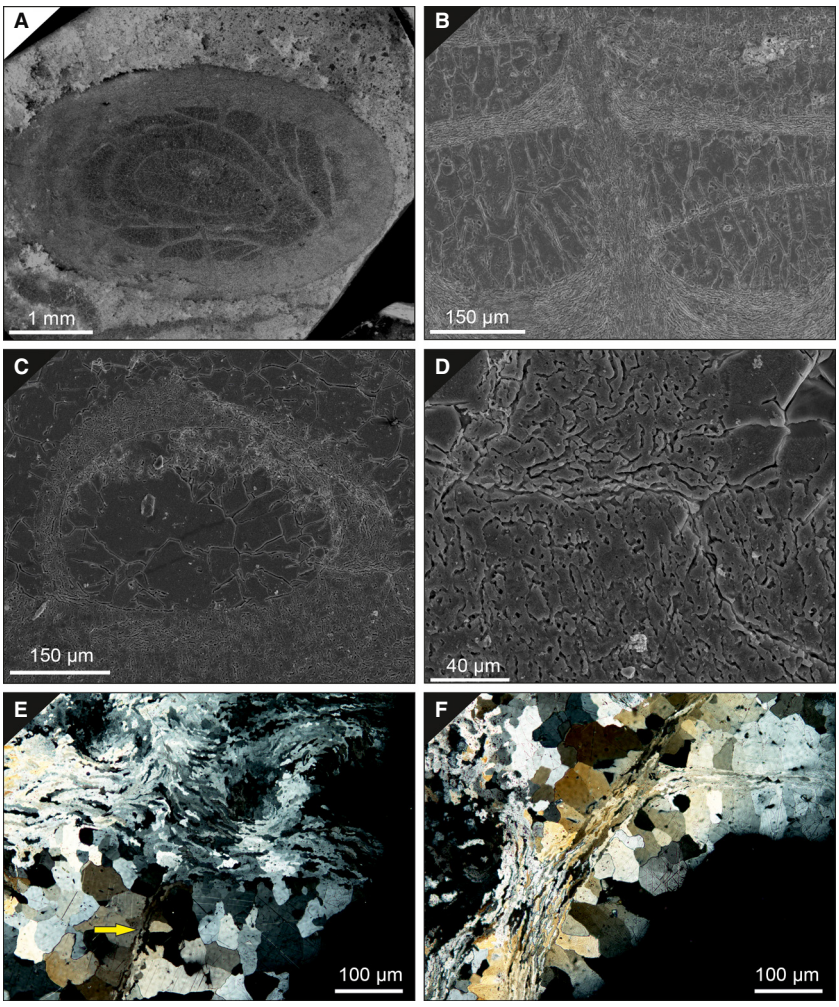

FIG. 9. A–B, SEM images of *Syringopora* sp.; A, transverse section, showing the inner structure of the tabularium; B, detail of a holacanth septal spine; note that two tabulae are cut by the spine, and the rotation of lamellae in the tabulae adapting to the morphological and crystallographic axis of fibres of the septal spine. C–D, SEM images of *Multithecopora* sp. C showing the contact of a coral wall and a tabula; C, note the contact zone of the inner fibrous domain and the lamellae of the tabulae at two points; D, detail of the contact area between the inner fibrous domains and the lamellae of the tabulae; note the fast rotation of lamellae that are adapting to the crystallographic axis between both elements. E–F, petrographic images of ultrathin sections of *Syringopora* sp.; E, detail of a tabula (arrow) which reaches the coral wall; note the tangential section of the coral and the 'egg-box' structure formed by the surrounding lamellae around the septal spines; the septal spines are anchored to the external edge of the coral wall; F, detail of the initiation of a tabula and the bifurcation of another; note the difference between the interference colours showing a new crystallographic orientation.

Figure 11 shows the peripheral origin on a microlamellae wall, and several crystallographic domains can be observed. A main microlamellae domain, with a morphological axis tilted obliquely to the growth direction, with a pole maxima in the {0001} plane completely inclined, is characteristic of transverse sections. Microlamellae show the *c*-axis directed towards the peripheral origin of tabula and turbostratic distribution (Fig. 5C). Gradually, crystals change their orientation, folding and turning to lamellae laterally, in a gradual change from lamellae of the wall to lamellae of the tabula, generating a new domain. Also, irregular sections of microlamellae are observed, wider than longer with the *c*-axis oriented towards the lumen, but downward in this section. The lamellae of the tabula, similar to lamellae on a transverse section of the coral wall, display a unique pole maximum on the {0001} plane. A perpendicular section should reflect the orientation of the lamellae, as in a longitudinal section, with the *c*-axis oriented perpendicular to orientation of tabulae. Probably, these changes in the *c*-axis position are due to changes in the position of the basal ectoderm that generated the lamellae. The lamellae of tabulae also have a turbostratic distribution, and their misorientations are similar to those of the wall, with modes around 5°, ~22°, ~5°, ~45° and ~60°, and they are tilted ~90° relative to microlamellae of the coral wall.

SEM observations have allowed visualization of the processes by which the tabulae intersected septal spines. In Figure 9, a holacanth spine of *Syringopora* sp. can be observed cutting two tabulae (Fig. 9B). At the point of contact, the lamellae change their orientation folding the crystal and surrounding the spine, as occurs in the wall where the lamellae are covering the spines. This process, as in *Multithecopora* sp. A, leads to an alignment of the *c*-axis between the lamellae and fibres, which indicates that both elements nucleated at the same time. Ultrathin sections in a longitudinal transect of *Syringopora* sp. (Fig. 9E–F) show that the tabulae can bifurcate. In this process, the crystals experience a branch-off at the inflexion point, in which there is a cluster of crystals that have the same crystallographic orientation, as shown by the interference colours under crossed polarizers. The new tabula shows a different

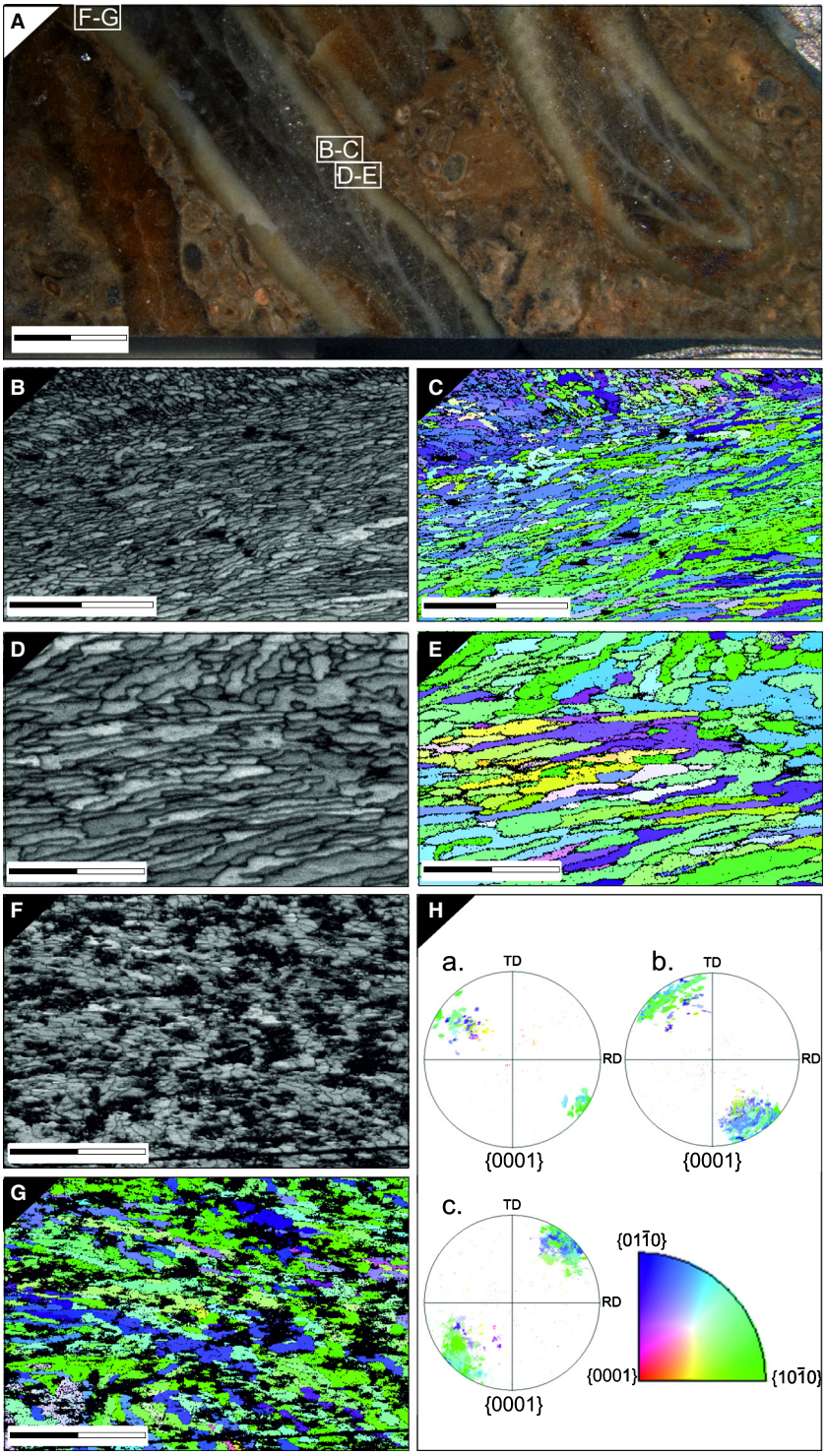

FIG. 10. *Syringopora* sp. A, two longitudinal sections of the skeleton and the location of the EBSD maps (white rectangles). B–C, EBSD images showing crystallography of the coral wall in a longitudinal section of a corallite; B, index intensity map, showing the structure of transition between lamellar and fibrous inner domains of the coral wall; C, crystallographic orientation map, showing the main crystallographic orientations of lamellae of the coral wall; note the gradual transition between fibres and lamellae. D–E, EBSD images showing crystallography of large scale of lamellae in the coral wall; note the nondiffraction in the contact of crystals and the co-orientation between some of them; D, index intensity map; E, crystallographic orientation map. F–G, EBSD images showing crystallography of a lamellar domain where dissolution by diagenesis is evident; F, index intensity map; G, crystallographic orientation map. H, pole figures (in normal direction view (ND) to the sample surface in a three axes reference system with indication of the reference (RD) and transverse (TD) directions) indicating crystallographic orientation of calcite crystals with reference to the *c*-axis; and crystallographic key indicating colour coding of crystallographic axes; a, orientations of lamellae of coral wall in D–E; b, orientation distribution of B–C; c, orientation distribution of F–G; note the random orientations of crystals in the diagenetic alteration zone inside of the pores. Scale bars represent 2 mm (A); 50 μm (B–C); 20 μm (D–E); and 25 μm (F–G).

crystallographic orientation, with respect to the parent tabula with dissimilar interference colours. Figure 9C–D shows a transverse section of *Multithecopora* sp. C, in which there are two points where a tabula is attached to the inner fibrous domain. At these points, the lamellae cover the fibres in the contact zone. The *c*-axis in the lamellae is perpendicular to the morphological axis and parallel to the fibres. Therefore, in these regions where the fibres and lamellae are merged in tabulae, both elements keep the same orientation. Subsequently, the lamellae change the direction of morphological axis towards the tabula during development.

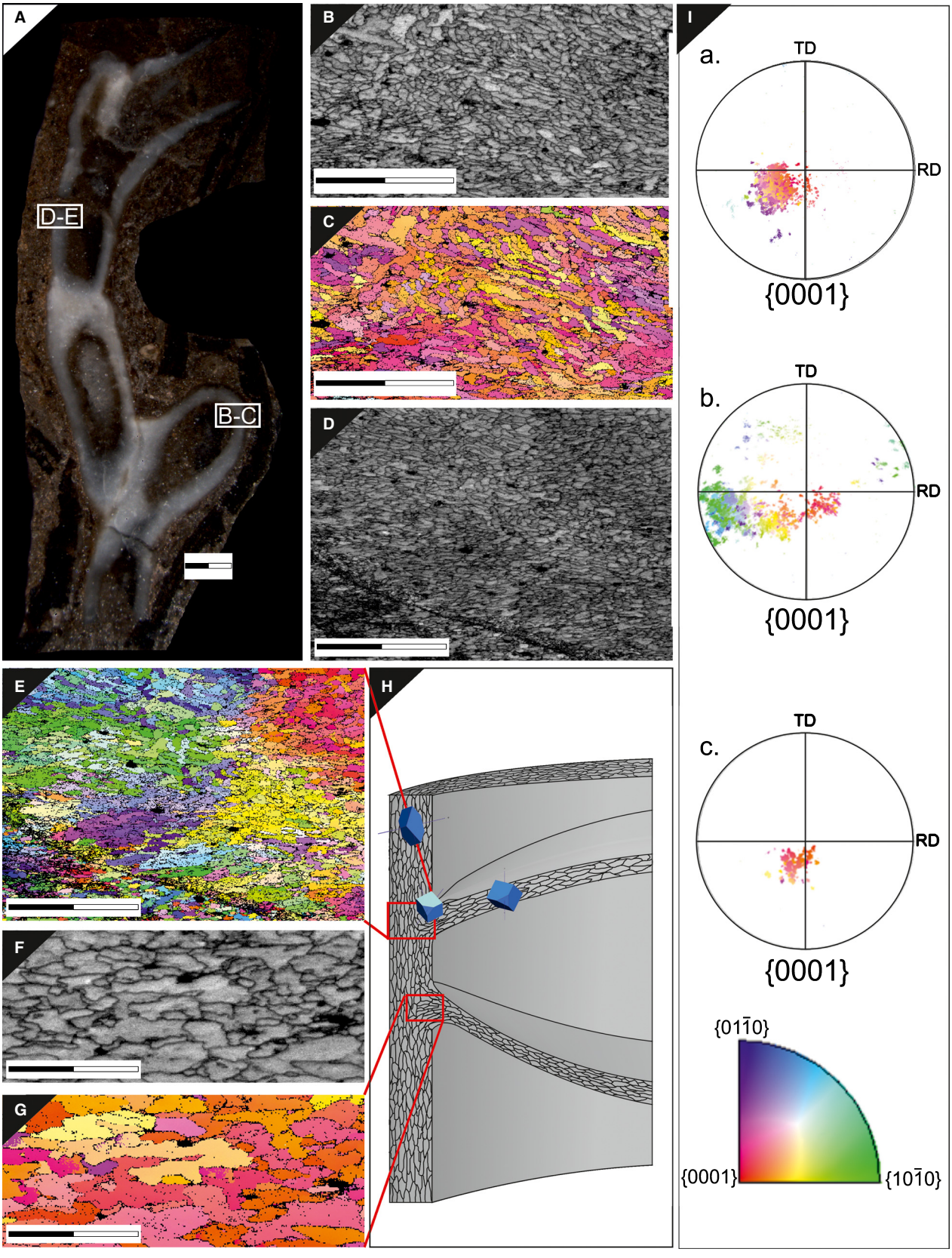
A
D-E
B-C
B
C
D
E
F
G
H
I
a.
TD
RD
{0001}
b.
TD
RD
{0001}
c.
TD
RD
{0001}
{01$\bar{1}$0}
{0001}
{10$\bar{1}$0}

Shared walls. The last wall element to be analysed was the shared walls in massive corals (cerioid or pseudocerioid corals), but this element is not a wall element *sensu stricto*. There are numerous articles that refer to it as the median lamina or dark lamina (Nicholson 1879; Plusquellec 1976; Plusquellec and Tchudinova 1977; Lafuste *et al.* 1992). This is a lamina of granules situated between the walls of two corallites in a massive colony; its origin is unknown. It was studied on a transverse section of *Roemeripora* sp. (Fig. 12). The EBSD map shows different regions that make up the shared wall of two corallites (Fig. 12E–F). An upper region can be recognized, formed by a microlamellae sclerenchyma, which shows mainly orientations in rows, arising from an irregular granular middle zone (median lamina). In the lower part, there is a microlamellae region more heterogeneous in crystallographic orientations. The upper microlamellae region has the *c*-axis oriented transversely with direction towards the lumen and the microlamellae and rows with orientation relative to fibres. The lower microlamellae region has an orientation oblique to the *c*-axis, opposite to the upper region (Fig. 12G), with direction of *c*-axis to the external wall. The *c*-axis is misoriented 40° between both walls. The middle region has the *c*-axis almost perpendicular to the growth direction. In the plane $\{10\bar{1}0\}$, six cluster of orientations are observed, each at 15°. The distribution of the orientations in the $\{10\bar{1}4\}, \{01\bar{1}8\}$ and $\{10\bar{1}8\}$ planes shows preferred orientations in the three main pole maxima of the calcite, but not a turbostratic distribution (Fig. 5). The misorientation differs between the different zones (Fig. S1). In the lower microlamellae zones, the misorientation is ~5°, 15°, 25° and 55°, whereas in the upper region it is ~5°, 13°, 15°, 25° and 40°, and finally, within the median lamina, it is ~5°, 13°,16°, 20°, 25°, 35°, 65° and 75°. Ultrathin section and SEM images of *Roemeripora* sp. colonies show that the median lamina has an undulose trajectory, occasionally incomplete, probably formed by the development of connecting pores between two corallites (Fig. 6). Ultrathin sections show that the divergence between the orientations is also recognized by the interference colour and the difference between the three zones is stronger (upper, lower and median lamina; Fig. 6E–H). These features seem to indicate that the median lamina was developed by the two corallites at the same time, sharing the biocrystallization process at this location.

DISCUSSION AND CONCLUSIONS

Growth patterns

Syringoporicae have an open calyx at the distal point of each corallite (Fig. 11 and Fig. S2), which does not exhibit the same thickness as the rest of the coral wall. This aperture suggests a noncontinuous growth mode at both edges of the wall (inner and external). The cylindrical corallites terminate in an open space where the polyp lived. This part can be closed at the bottom by a basal tabula, of any morphology, where the polyp was supported, or even septal spines surrounding the calyx. The wall is characterized by having a wedge-shaped ending opening to the outside. The continuous transition between domains (lamellae to fibres, where it exists) and between different crystals suggests that the nucleation of crystals could be accomplished by the same epithelial cells, without a distinction between layers. The epithelium would have surrounded the inner edge of the calyx, and the highest and lowest points of the wall would have been formed at the same time in the calyx (Fig. S2). This structure indicates that the growth direction is divided into two main components, a horizontal growth direction towards the lumen and a vertical direction towards the outside (Fig. S2). In the case of cerioid or pseudocerioid corals, such as *Roemeripora* sp., the granules of the median lamina begin to form before the lamellae in both cor-

FIG. 11. *Sinopora* sp. A, longitudinal section of the skeleton and location of the EBSD maps (white rectangles); note the open calyx at the end of the colony. B–C, EBSD images showing crystallography of the coral wall in transverse section of a corallite; B, index intensity map, showing the lamellar tissue of the coral wall; C, crystallographic orientation map, showing the main crystallographic orientations of the coral wall. D–E, EBSD images showing crystallography of the peripheral origin of tabulae; D, index intensity map, showing the lamellar structure of the coral wall and the progressive change of microcrystalline texture of the peripheral origin of tabulae; E, crystallographic orientation map, showing the main crystallographic orientations in the peripheral origin of tabula; note the colours of different regions adapting the orientation to the tabula. F–G, EBSD image showing crystallography of the inner zone of the same tabula; F, index intensity map, showing the irregular lamellar structure of the beginning of the tabula; G, crystallographic orientation map, showing the main crystallographic orientations of the lamellae of tabulae. H, 3D interpretative sketch of the peripheral origin of tabula in a coral wall; note the theoretical rhombohedra and their rotation at the different points analysed by EBSD in *Sinopora* sp. I, pole figures (in normal direction view (ND) to the sample surface in a three axes reference system with indication of the reference (RD) and transverse (TD) directions) indicating the crystallographic orientation of calcite crystals with reference to the *c*-axes, and crystallographic key indicating the colour coding of crystallographic axes; a, orientations of lamellae of coral wall in B–C; b, orientation distribution of D–E; note the rotation of orientations from coral wall to the tabula; c, detail of orientation of *c*-axis of tabula. Scale bars represent 1 mm (A), 70 μm (B–E) and 25 μm (F–G).

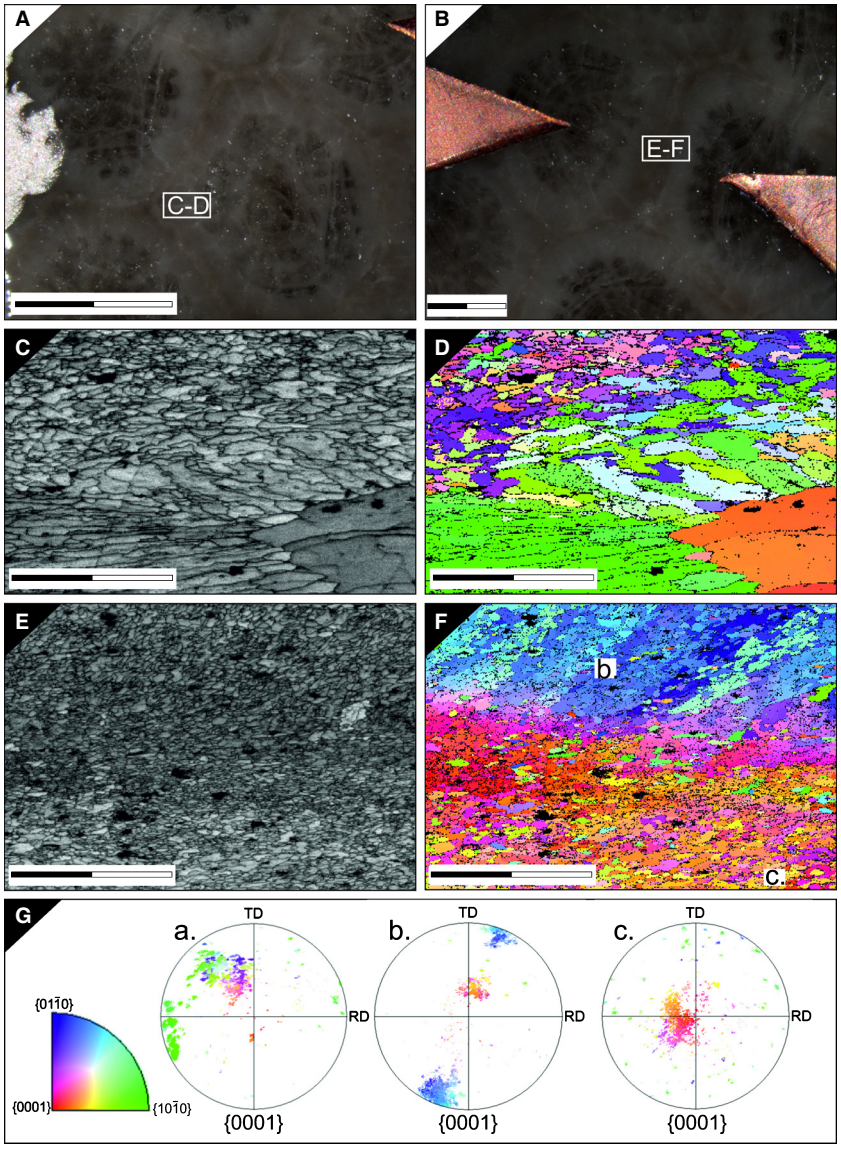

FIG. 12. A–B, Two transverse sections of the skeleton of *Roemeripora* sp. and location of the EBSD maps (white rectangles). C–D, EBSD images showing crystallography of the inflexion point in the coral wall; C, index intensity map, showing the structure of the transition between the lamellar and fibrous inner domains of the coral wall; D, crystallographic orientation map; note the gradual transition between fibres and lamellae in the same side of the corallite. E–F, EBSD images showing crystallography of a shared wall in *Roemeripora* sp.; note the median line between two corallites and the lamellar domain of the upper region, which is reminiscent of fibres; E, index intensity map; F, crystallographic orientation map; b and c correspond to the pole figures shown in G. G, pole figures (in normal direction view (ND) to the sample surface in a three axes reference system with indication of the reference (RD) and transverse (TD) directions) indicating crystallographic orientation of calcite crystals with reference to the *c*-axis and crystallographic key indicating colour coding of crystallographic axes; a, orientations of fibres and lamellae of the coral wall in C–D; note the rotation of ~60° between the crystallographic elements on both sides of the polygonal corallite; b, orientation distribution of lamellae of upper region of E–F; note the longitudinal disposition of lamellae (blue dots) versus the median lamina; c, orientation distribution of lamellae of the lower region on the other side of the shared wall; note that these crystals are disposed in a quasi-vertical fashion. Scale bars represent 1 mm (A–B); 45 μm (C–D); and 70 μm (E–F).

allites, because they share preferred crystallographic orientations.

EBSD maps (Figs 7, 8, 10–13) and ultrathin sections (Figs 4, 6) indicate that some crystals, both in lamellae and fibres of the seven taxa analysed in this study, have similar orientation (co-orientation) and usually form a package of crystals with a stepped pattern of growth and a main misorientation among crystals of less than 5°. This

package of co-oriented crystals is cut by another package of crystals that have a different co-orientation, but in the coral wall appear laterally as crystals with the same orientation. In the contact zone between crystals, there is a region in the EBSD maps with no diffraction, which indicates another mineral phase different to calcite, or a non-crystalline phase. These nondiffracting areas in EBSD have been interpreted as corresponding to the organic matrix, because the organic template between the crystals is usually closed in recent carbonate skeletons (Checa *et al.* 2006; Goetz *et al.* 2009, 2011; Perez-Huerta *et al.* 2011). Ultrathin sections show a black cortex around some crystals and occasionally black spots inside the crystals (both isotropic). SEM images show that after acid etching, the shape and contour of the crystals can be observed, reflecting deeper lines around the crystals and dissolution gulfs inside them. These facets point to the existence of organic matter remaining in the walls of the Syringoporicae. This was described by Lafuste and Tourneur (1991) in other tabulate corals and has been suggested for *Multithecopora hontoriense* (Coronado *et al.* 2013).

An additional point of consideration is the growth of lamellae and fibres in both sections with different sizes and outlines, as summarized in Table 1. The direction of the *c*-axis is maintained during growth, and differences are observed along the *a*- and *b*-axes, which are rotated. If the packages of crystals conserve the same preferred crystallographic orientation, and the different sizes and outlines of crystals, it could be suggested that both lamellae and fibres could be involved in competitive growth, being limited by the size of contact with other crystals or packages (Rodríguez-Navarro and García-Ruíz 2000; Dalbeck and Cusack 2006; Schmahl 2010). Different mathematical algorithms have been developed for describing this growth, but applying them to microstructures of fossil cnidarians is difficult, due to the problems of establishing a base line in the growth of the crystals in a stepped pattern mode of development.

Biogenic origin of microstructures in Syringoporicae

There is a long-standing controversy about the origin, biogenic or diagenetic, of structural elements in Palaeozoic corals, even regarding the presence of the original mineral phase (Kato 1963; Sorauf 1971, 1978, 1983; Oekentorp 1984, 2001; Lafuste and Plusquellec 1985; Rodríguez 1989; Falces 1997). In this study, seven taxa of Palaeozoic tabulate corals show a common calcitic biocrystallization process based on crystallographic observations, highlighting the biogenic origin of these microstructures, as previously indicated by Coronado *et al.* (2013). The microstructure of Syringoporicae can be formed by lamellae, fibres, granules or by a combination of these. The transition or change between the different morphological elements is gradual, as was indicated previously by Lafuste (1978, 1983), and the *c*-axis is always oriented parallel to the growth of lamellae and fibres, as was observed in the petrographic microscopy study of Fischer and Lafuste (1972), suggesting a growth model without a specific layer of epicellular tissue. All the taxa studied here have a common biocrystallization process resulting in a shared misorientation pattern. This pattern is only altered when the wall elements modify the position of crystalline elements. Similar to other organisms secreting calcium carbonate biominerals, the most common misorientation is less than 5° (Dalbeck and Cusack 2006), which suggests a common strategy of nucleation for these elements.

Wall elements have also a common misorientation, and even where they have a different structure, reflecting a common strategy of growth, as, for example, in the tabulae or septal spines. These properties confirm a biogenic origin of these elements and microstructures, but also a common genetic inheritance. The difference in the building of these elements and their position in the wall probably were conditioned by the protean nature of the organic matrix in these regions, which exerted a stronger control in the crystallization of these elements. Some orientations of wall elements and crystals are highlighted against the main organization of the skeleton. Interestingly, the holacanth spines show a turn in *a*- and *b*-axes at their base and sometimes, starting at the beginning of the wall (external part). This character could have a physiological explanation, due, perhaps, to the septal spines clamping to the polyp or by their retractable movement under high turbulence currents. On the other hand, tabulae have a disposition of *c*-axis perpendicular to the growth direction. Originally, Tchudinova (1986) established that the microstructure of tabulae in the Syringoporicae was fibrous, but EBSD data reveal that it is in fact lamellar. The disposition of the tabulae probably supported the polyp in the vertical direction, and the *c*-axis of tabulae is oriented perpendicular to the growth direction.

As in other calcitic groups of organisms, the orientations and relationships between crystallographic elements of the skeletons of Syringoporicae show a distribution and misorientation that would prevent skeleton fracture by cleavage. Calcite crystals are easily cleaved on their $\{10\bar{1}4\}$ planes (Schmahl *et al.* 2004). The skeletons of the Syringoporicae have the *c*-axis oriented perpendicular to the growth direction, protecting the skeleton from lateral currents of seawater. Turbostratic distribution, which is a rotation of *a*- and *b*-axes around the *c*-axis, could be a strategy to prevent cleavage in Syringoporicae, and it would represent an evolutionary advantage for this coral group that inhabited

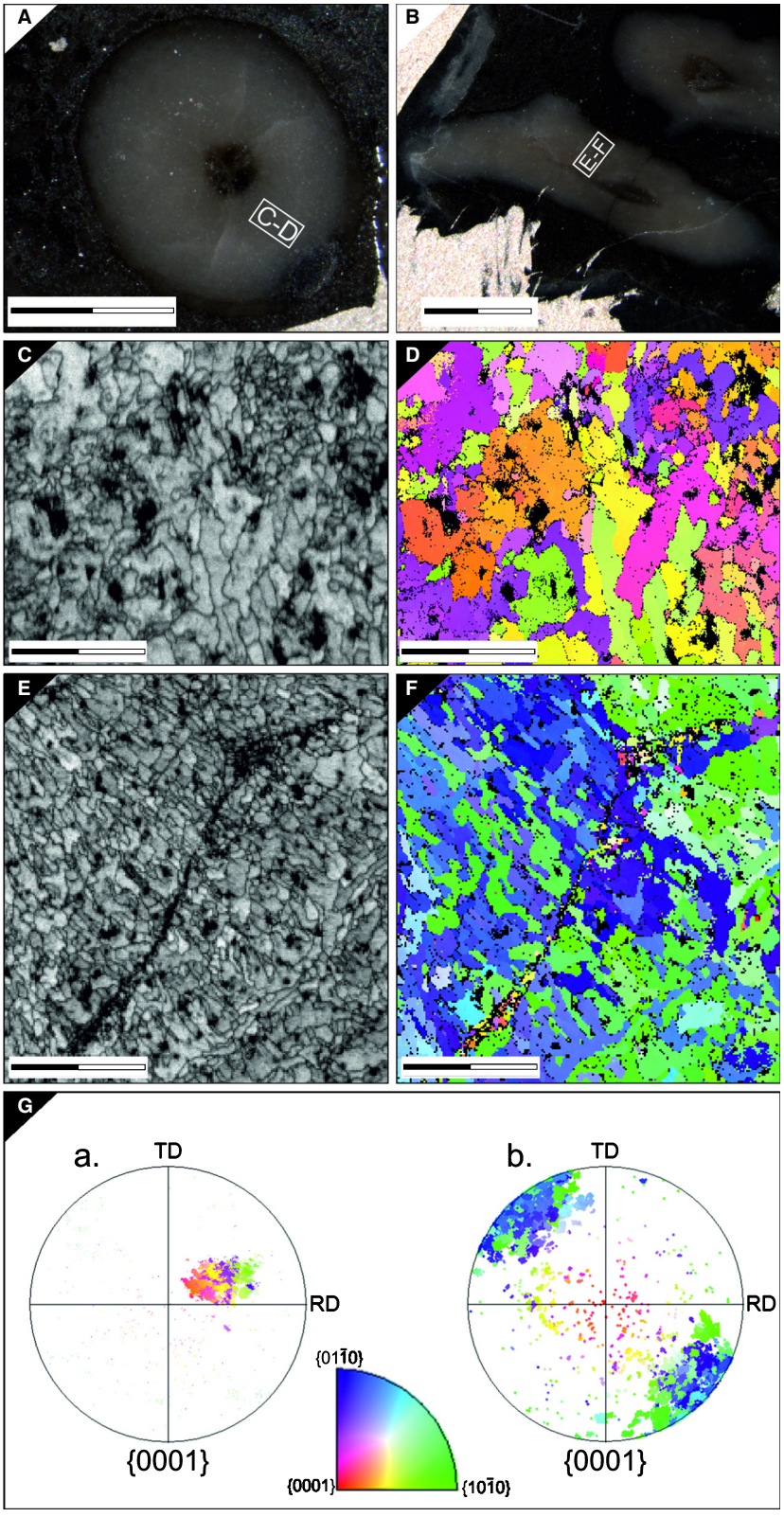

FIG. 13. A, transverse and, B, longitudinal sections of the skeleton of *Multithecopora* sp. D and location of the EBSD maps (white rectangles). C–D, EBSD images showing crystallography of a coral wall in a transverse section of a corallite. C, index intensity map, showing the structure of transition from lamellar to fibrous domains of a coral wall; D, crystallographic orientation map, showing the main crystallographic orientations of lamellae of the coral wall. E–F, EBSD images of small scale of transition between lamellae of the external domain and fibres of the inner domain; E, index intensity map, showing the fibrous structure of a coral cut by a microfracture; note the dark coloration of the microfracture and the porosity (black spots) associated with this event; F, crystallographic orientation map, showing the main crystallographic orientations in the transition between domains; note the different colours of crystals of the microfracture. G, pole figures (in normal direction view (ND) to the sample surface in a three axes reference system with indication of the reference (RD) and transverse (TD) directions) indicating the crystallographic orientation of calcite crystals with reference to the c-axes; and a crystallographic key indicating colour coding of crystallographic axes.; a, orientations of lamellae of a coral wall in C–D; b, orientation distribution of E–F; note the random orientations of crystals in the diagenetic alteration zone. Scale bars represent 1 mm (A); 2 mm (B); 50 μm (C–D); and 100 μm (E–F).

different marine environments during the Palaeozoic. Turbostratic distribution has been detected in other invertebrates, for example, in the foliated calcite of bivalves (*Pecten maximus*; Checa *et al.* 2007), and it could be a common biomineralization strategy to prevent fracture by cleavage. This misorientation pattern has also been

observed in the outer prismatic layer of *Mytilus edulis* (Dalbeck and Cusack 2006). Both *Pecten maximus* and *Mytilus edulis* live in circumlittoral regions where their shells are subject to changes in the energy of tides and waves. This fact might explain that this crystallographic distribution could be an advantage for the Syringoporicae. As explained before, the modification of the growth of skeletons by wall elements could modify biocrystallization processes at a family level. An example of this is the massive skeleton of *Roemeripora* sp. that does not show a turbostratic crystallographic distribution. Instead, the morphology of corallites (pseudohexagonal shaped or honeycomb shaped) seems to have a macroscale strategy to avoid fracture by cleavage, because the orientation of the *c*-axis in a wall of a corallite is the same and without inner rotation as occurs in phaceloid corals. The *c*-axis is rotated ~60° with respect to the centre of polyp in each wall (Fig. 6A). The disposition of the *c*-axis in shared walls of *Roemeripora* sp. shows that it is misorientated 40° between the two walls. This arrangement could protect the skeletons against fractures, developing the colony as a single organism to deal with strong marine currents.

Coordinated stepping growth mode and mineral bridges

Cuif *et al.* (2012) reviewed the calcium carbonate skeletogenesis of different organisms showing that the growth patterns of molluscs and Recent corals converge. They observed that these organisms have a coordinated step growth that begins with the secretion of an organic gel layer, where the insoluble organic matrix acts as a site of crystallization. As a consequence of this process, mineral phases show a specific reticulate pattern, formed by strongly packed and fused units built by superposition of mineralized layers, basically continuous between neighbouring units, with an irregular organic-rich coating around them.

Results herein point to a mode of growth of the Syringoporicae convergent with and equivalent to other mineralizing organisms secreting calcium carbonate. The formation of lamellae and fibres could be mediated by an organic layer that controlled the beginning and end of growth of crystal units. The evidence for an organic matrix, at both the nanoscale and microscale, was suggested by Coronado *et al.* (2013) and is further supported by EBSD data in this study. The organization of co-oriented crystals in packages and the distribution of different packages in the three dimensions of space support this coordinated step growth model. All observations indicate that crystals with the same orientation (or package) were nucleated in contact with another, maintaining the preferred crystallographic orientations during the process of growth. This could indicate that the crystals grew by heteroepitaxy, as previously suggested for the formation of aragonite nacre (Weiner and Traub 1980, 1981), although recent studies have shown that the nacre growth is produced by mineral bridges (Checa *et al.* 2011). The mineral bridge hypothesis was developed by Wada (1972) through a model of connections between tablets in bivalves across the interlamellar membranes. Previous studies using different techniques in molluscs showed that nacre tablets are stacked along a single column illustrating that they are co-oriented (Dimasi and Sarikaya 2004; Dalbeck and Cusack 2006; England *et al.* 2007; Checa *et al.* 2011). From these studies, two different facts emerge about what is required to establish the presence of a mineral bridge (Checa *et al.* 2011): (1) crystals in direct continuity should be co-orientated; and (2) there must be an intercrystalline membrane at the contact between crystals.

Lamella and fibre packages, as described in this study, show that the crystals are co-orientated and that there can be a discontinuous intercrystalline organic membrane. Inside the packages, the crystallographic orientation is continuous across the lamellae and fibres, which suggests that the crystals of each package could have nucleated by the mechanism of mineral bridges. The packages in representatives of Syringoporicae have an irregular or dendritic growth that differs from the regular growth of nacre in columns or rows.

The variability in the shapes and sizes of crystals, and the gradual transition from lamellae to fibres in representatives of the Syringoporicae, suggest that the proteins responsible for growth exerted a control different to that in molluscs and brachiopods, in which there can be different organic components between the layers (Checa *et al.* 2006; England *et al.* 2007; Goetz *et al.* 2009, 2011). Nucleation in representatives of the Syringoporicae should take part, as a hierarchical response, within the template of organic matter secreted by the ectodermal layer, in which, at a nanoscale level, the nano-units were nucleated with an orientation towards the *c*-axis, forming a biocomposite (Coronado *et al.* 2013). The biocomposite forms a microcrystal, and other co-oriented microcrystals are formed during nucleation, by a mechanism similar to mineral bridges, creating a package. Each microcrystal and package seems to have grown in a competitive growth mode with other crystals, due to the variability of sizes and morphologies.

Future research will compare these observations with older syringoporoids and other groups of tabulate and rugose corals.

Acknowledgements. Financial support through the Spanish Ministerio de Economía y Competitividad (research project CGL2012-30922BTE) and Complutense University Research Group (910231) is gratefully acknowledged. IC acknowledges financial support through a FPI-UCM 2 Grant and the Synthesis

Grant. This article is a contribution to the Spanish Working Group IGCP 596 *Climate change and biodiversity patterns in the Mid-Palaeozoic* (UNESCO). We sincerely thank the staff of Research Assistance Centre of Geological Techniques (Universidad Complutense of Madrid, Spain). A.P-H. thanks the College of Arts & Sciences (The University of Alabama) for support and Johnny Goodwing (CAF) for help with SEM. We also give our sincere thanks to Ian D. Somerville (UCD) for his advice and the English revision of the manuscript. We thank the reviewers (Bruno Mistiaen and anonymous) and the editors (George Sevastopulo and Sally Thomas) for their help, constructive comments and the English style of the text.

Editor. George Sevastopulo

SUPPORTING INFORMATION

Additional Supporting Information may be found in the online version of this article:

Appendix S1. Methods.
Figure S1. Misorientation histograms.
Figure S2. Calyx formation.
Table S1. Main taxonomical characters.

REFERENCES

BACHMANN, F., HIELSCHER, R. and SCHAEBEN, H. 2011. Grain detection from 2d and 3d EBSD data—specification of the MTEX algorithm. *Ultramicroscopy*, **111**, 1720–1733.

BALTHASAR, U., CUSACK, M., FARYMA, L., CHUNG, P., HOLMER, L. E., JIN, J., PERCIVAL, I. G. and POPOV, L. E. 2011. Relic aragonite from Ordovician–Silurian brachiopods: implications for the evolution of calcification. *Geology*, **39**, 967–970.

CHECA, A. G. and RODRÍGUEZ-NAVARRO, A. B. 2005. Self-organisation of nacre in the shells of Pterioida (Bivalvia: Mollusca). *Biomaterials*, **26**, 1071–1079.

—— OKAMOTO, T. and RAMIREZ, J. 2006. Organization pattern of nacre in Pteriidae (Bivalvia: Mollusca) explained by crystal competition. *Proceedings of the Royal Society of London, Series B: Biological Sciences*, **273**, 1329–1337.

—— ESTEBAN-DELGADO, F. J. and RODRÍGUEZ-NAVARRO, A. B. 2007. Crystallographic structure of the foliated calcite of bivalves. *Journal of Structural Biology*, **157**, 393–402.

—— RAMIREZ-RICO, J., GONZALEZ-SEGURA, A. and SANCHEZ-NAVAS, A. 2009. Nacre and false nacre (foliated aragonite) in extant monoplacophorans (=Tryblidiida: Mollusca). *Naturwissenschaften*, **96**, 111–122.

—— CARTWRIGHT, J. H. E. and WILLINGER, M.-G. 2011. Mineral bridges in nacre. *Journal of Structural Biology*, **176**, 330–339.

COLMENERO, J. R., FERNANDEZ, L. P., MORENO, C., BAHAMONDE, J. R., BARBA, P., HEREDIA, N. and GONZALEZ, F. 2002. Carboniferous. 93–116. *In* GIBBONS, W. and MORENO, T. (eds). *The geology of Spain*. Geological Society, London, 632 pp.

CORONADO, I. and RODRÍGUEZ, S. 2014. Carboniferous auloporids from the Iberian Peninsula: palaeoecology, diversity, and spatio-temporal distribution. *Journal of Iberian Geology*, **40**, 61–85.

—— PÉREZ-HUERTA, A. and RODRÍGUEZ, S. 2013. Primary biogenic skeletal structures in Multithecopora (Tabulata, Pennsylvanian). *Palaeogeography, Palaeoclimatology, Palaeoecology*, **386**, 286–299.

CUIF, J.-P., DAUPHIN, Y., NEHRKE, G., NOUET, J. and PEREZ-HUERTA, A. 2012. Layered growth and crystallization in calcareous biominerals: impact of structural and chemical evidence on two major concepts in invertebrate biomineralization studies. *Minerals*, **2**, 11–39.

CUSACK, M. and WILLIAMS, A. 2001. Evolutionary and diagenetic changes in the chemico-structure of the shell of cranioid brachiopods. *Palaeontology*, **44**, 875–903.

—— ENGLAND, J., DALBECK, P., TUDHOPE, A. W., FALLICK, A. E. and ALLISON, N. 2008. Electron backscatter diffraction (EBSD) as a tool for detection of coral diagenesis. *Coral Reefs*, **27**, 905–911.

—— GUO, D., CHUNG, P. and KAMENOS, N. A. 2013. Biomineral repair of abalone shell apertures. *Journal of Structural Biology*, **183**, 165–171.

DALBECK, P. and CUSACK, M. 2006. Crystallography (electron backscatter diffraction) and chemistry (electron probe microanalysis) of the avian eggshell. *Crystal Growth & Design*, **6**, 2558–2562.

—— —— DOBSON, P. S., ALLISON, N., FALLICK, A. E. and TUDHOPE, A. W. 2011. Identification and composition of secondary meniscus calcite in fossil coral and the effect on predicted sea surface temperature. *Chemical Geology*, **280**, 314–322.

DIMASI, E. and SARIKAYA, M. 2004. Synchrotron x-ray microbeam diffraction from abalone shell. *Journal of Materials Research*, **19**, 1471–1476.

ENGLAND, J., CUSACK, M., DALBECK, P. and PÉREZ-HUERTA, A. 2007. Comparison of the crystallographic structure of semi nacre and nacre by electron backscatter diffraction. *Crystal Growth & Design*, **7**, 307–310.

FALCES, S. 1997. Borings, embeddings and pathologies against microstructure. New evidences on the nature of the microstructural elements in rugose corals. *Boletín de la Real Sociedad Española de Historia Natural (Geologia)*, **92**, 96–116.

—— and RODRÍGUEZ, S. 1999. Observations on the skeletogenesis of rugose corals. *Abstracts of the 8th International Symposium on Fossil Cnidaria and Porifera, September 12–16, 1999, Sendai, Japan,* **44**.

FEDOROWSKI, J. 2001. Upper Palaeozoic coral studies: where we are and where we should be. *Bulletin of Tohoku University Museum*, **1**, 1–6.

—— 2010. Remarks on rugose coral taxonomy. *Palaeoworld*, **19**, 242–248.

FISCHER, J.-C. and LAFUSTE, J. 1972. Nouvelles observations sur la paléohistologie du genre *Acanthochaetetes* (Hydrozoa, Chaetetida). *Bulletin de la Société Géologique de France*, Series 7, **XIV**, 320–324.

FRANK, F. C. and MEDALIST, F. M. 1988. Orientation mapping. *Metallurgical Transactions A*, **19**, 403–408.

GOETZ, A. J., GRIESSHABER, E., NEUSER, R. D., LÜTER, C., HÜHNER, M., HARPER, E. and SCHMAHL, W. W. 2009. Calcite morphology, texture and hardness in the distinct layers of rhynchonelliform brachiopod shells. *European Journal of Mineralogy*, **21**, 303–315.

—— STEINMETZ, D. R., GRIESSHABER, E., ZAEFFERER, S., RAABE, D., KELM, K., IRSEN, S., SEHRBROCK, A. and SCHMAHL, W. W. 2011. Interdigitating biocalcite dendrites form a 3-D jigsaw structure in brachiopod shells. *Acta Biomaterialia*, **7**, 2237–2243.

GRELLET-TINNER, G., SIM, C. M., KIM, D. H., TRIMBY, P., HIGA, A., AN, S. L., OH, H. S., KIM, T. J. and KARDJILOV, N. 2011. Description of the first lithostrotian titanosaur embryo in ovo with Neutron characterization and implications for lithostrotian Aptian migration and dispersion. *Gondwana Research*, **20**, 621–629.

HILL, D. 1981. Rugosa and Tabulata. 1–762. *In* TEICHERT, C. (ed.). *Treatise on invertebrate paleontology, Part F, Coelenterata, Suppl. 1*. Geological Society of America, Boulder, CO and University of Kansas Press, Lawrence, KS, 762 pp.

KAMINSKY, W. 2007. From CIF to virtual morphology using the WinXMorph program. *Journal of Applied Crystallography*, **40**, 382–385.

KATO, M. 1963. Fine skeletal structures in Rugosa. *Journal of the Faculty of Science, Hokkaido University*, Series 4, **11**, 571–630.

LAFUSTE, J. 1970. Lames ultra-minces à faces polies. Procedé et Application à la microstructure des Madréporaires fossiles. *Comptes Rendus Hebdomadaires des Séances de l'Académie des Sciences, Paris*, **270**, 679–681.

—— 1978. Modalités de passage des lamelles aux fibres dans la muraille de Tabulés (Micheliniidae) du Dévonien et du Permien. *Geobios*, **11**, 405–408.

—— 1981. Structure et microstructure de *Dendropora* Michelin 1846 (Tabulata, Dévonien). *Bulletin de la Société Géologique de France*, **23**, 271–277.

—— 1983. Passage des microlamelles aux fibres dans le squelette d'un Tabulé 'michelinimorphe' du Viséen du Sahara algérien. *Geobios*, **16**, 755–761.

—— and PLUSQUELLEC, Y. 1985. Attribution de '*Michelinia*' *compressa* Michelin, 1847 au genre *Yavorskia* Fomitchev (Tabule, Tournaisien). *Geobios*, **18**, 381–387.

—— and TOURNEUR, F. 1991. Biocristaux et éléments foncés de la muraille chez Thamnopora Steininger, 1831 (Tabulata, Dévonien). *Annales de Paléontologie*, **77**, 3–20.

—— FERNÁNDEZ-MARTÍNEZ, E. and TOURNEUR, F. 1992. *Parastriatopora* (Tabulata) de las Calizas del Lorito (Devónico Inferior, provincia de Córdoba). *Revista Española de Paleontología*, **7**, 3–12.

LEE, M. R., TORNEY, C. and OWEN, A. W. 2007. Magnesium-rich intralensar structures in schizochroal trilobite eyes. *Palaeontology*, **50** (5), 1031–1037.

LOTZE, F. 1945. Zur gliederung der varisziden der iberischen Meseta. *Geotektonische Forschungen*, **6**, 78–92.

MORENO-AZANZA, M., MARIANI, E., BAULUZ, B. and CANUDO, J. I. 2013. Growth mechanisms in dinosaur eggshells: an insight from electron backscatter diffraction. *Journal of Vertebrate Paleontology*, **33**, 121–130.

NELSON, S. J. 1962. Analysis of Mississippian *Syringopora* from the southern Canadian Rocky Mountains. *Journal of Paleontology*, **36**, 442–460.

NICHOLSON, H. A. 1879. *On the structure and affinities of the 'tabulate corals' of the Palaeozoic period, with critical descriptions of illustrative species*. William Blackwood & Sons, Edinburgh & London, 342 pp.

OEKENTORP, K. 1984. Aragonite and diagenesis in Permian corals. *Palaeontographica Americana*, **54**, 282–292.

—— 2001. Review on diagenetic microstructures in fossil corals-a controversial discussion. *Bulletin of Tohoku University Museum*, **1**, 193–209.

OGILVIE, M. M. 1895. Microscopic and systematic study of madreporarian types of corals. [Abstract]. *Proceedings of the Royal Society of London*, **59**, 9–18.

PEREZ-HUERTA, A. and CUSACK, M. 2008. Common crystal nucleation mechanism in shell formation of two morphologically distinct calcite brachiopods. *Zoology (Jena)*, **111**, 9–15.

—— —— and ENGLAND J. 2007. Crystallography and diagenesis in fossil Craniid brachiopods. *Palaeontology*, **50**, 757–763.

—— DAUPHIN, Y., CUIF, J. P. and CUSACK, M. 2011. High resolution electron backscatter diffraction (EBSD) data from calcite biominerals in recent gastropod shells. *Micron*, **42**, 246–251.

—— CUSACK, M. and MÉNDEZ, C. A. 2012. Preliminary assessment of the use of electron backscatter diffraction (EBSD) in conodonts. *Lethaia*, **45**, 253–258.

PLUSQUELLEC, Y. 1976. Les polypiers. Tabulata. 183–215. *In* LARDEUX, H. (ed.). *Les Schistes et Calcaires éodévoniens de Saint-Cénéré (Massif Armoricain, France). Sédimentologie, paléontologie, stratigraphie.*. Mémoires de la Societé géologique et minéralogique de Bretagne, **19**, 323 pp.

—— and TCHUDINOVA, I. I. 1977. The microstructure of *Parastriatopora* Sokolov, 1949 (Siluro-Devonian Tabulata). *Annales de la Société Géologique du Nord*, **97**, 127–130.

RAJAN, K. 2000. Representations of Texture in Orientation Space. 31–38. *In* SCHWARTZ, A., KUMAR, M. and ADAMS, B. (eds). *Electron backscatter diffraction in materials science*. Springer, New York, 403 pp.

RODRÍGUEZ, S. 1989. Lamellar microstructure in Palaeozoic corals: origin and use in taxonomy. *Memoirs of the Association of Australasian Palaeontologists*, **8**, 157–168.

RODRÍGUEZ-NAVARRO, A. 2006. XRD2DScan: new software for polycrystalline materials characterization using two-dimensional X-ray diffraction. *Journal of Applied Crystallography*, **39**, 905–909.

—— and GARCÍA-RUÍZ, J. M. 2000. Model of textural development of layered crystal aggregates. *European Journal of Mineralogy*, **12**, 609–614.

SANDBERG, P. A. 1975. Bryozoan diagenesis; bearing on the nature of the original skeleton of rugose corals. *Journal of Paleontology*, **49**, 587–606.

SCHMAHL, W. W. 2010. The hierarchical organization in biomaterials: from nanoparticles via mesocrystals to function-

ality citation. 5–21. *In* FERNÁNDEZ DÍAZ, L. and ASTILLEROS GARCÍA-MONGE, J. M. (eds). *Biominerals and biomineralization processes*. Seminarios de la Sociedad Española de Mineralogía, **7**, Sociedad Española de Mineralogía, Madrid, 88 pp.

—— GRIESSHABER, E., NEUSER, R., LENZE, A., JOB, R. and BRAND, U. 2004. The microstructure of the fibrous layer of terebratulide brachiopod shell calcite. *European Journal of Mineralogy*, **16**, 693–697.

SEMENOFF-TIAN-CHANSKY, P. 1974. Données nouvelles sur la microstructure de certains Tétracoralliaires. 132–144. *In* SOKOLOV, B. (ed.). *Drevniye Cnidaria*. Proceedings of the 1st International Symposium on Fossil Cnidaria, Trudy Instituta Geologii i Geofiziki AN SSR, Sibirskoe Otdeleniye, **201**, 362 pp. [in French]

—— 1984. Microstructure of *Siphonodendron* (Lithostrotinidae). *Palaeontographica Americana*, **54**, 489–500.

SOKOLOV, B. S. 1947. Novye syringoporidy Taymyra. *Moskovskogo Obshchestva Ispytatelei Prirody, Byulletin (Geologiia)*, **22**, 19–28. [in Russian]

SORAUF, J. E. 1971. Microstructure in the exoskeleton of some Rugosa (Coelenterata). *Journal of Paleontology*, **45**, 23–31.

—— 1978. Original structure and composition of Permian rugose and Triassic scleractinian corals. *Palaeontology*, **21**, 321–339.

—— 1983. Primary biogenic structures and diagenetic history of *Timorphyllum wanneri* (Rugosa), Permian, Timor, Indonesia. *Memoirs of the Association of Australasian Palaeontologists*, **1**, 275–288.

—— 1984. Upper Permian corals from Timor and diagenesis. *Palaeontographica Americana*, **54**, 294–302.

STOLARSKI, J. and MAZUR, M. 2005. Nanostructure of biogenic versus abiogenic calcium carbonate crystals. *Acta Palaeontologica Polonica*, **50**, 847–865.

—— MEIBOM, A., PRZENIOSLO, R. and MAZUR, M. 2007. A cretaceous scleractinian coral with a calcitic skeleton. *Science*, **318**, 92–94.

STRUVE, A. 1898. Ein Beitrag zur Kenntnis des festen Gerüstes der Steinkorallen. *Verhandlungen der Russichen Kayser Mineralogischen Gessellschaft*, **2**, 43–116. [in German]

TCHUDINOVA, I. I. 1986. *Sostav, sistema i fllogenlya iskopayemykh korallov. Otryad Sirlngoporlda*, Vol. 216. Trudy Paleontologlcheskogo Instltuta Akad. Nauk URSS, 205 pp. [in Russian]

TORNEY, C., LEE, M. R. and OWEN, A. W. 2014. Microstructure and growth of the lenses of schizochroal trilobite eyes. *Palaeontology*, **57** (4), 783–799.

WADA, K. 1972. Nucleation and growth of aragonite crystals in the nacre of some bivalve molluscs. *Biomineralization*, **4**, 141–159.

WEINER, S. and TRAUB, W. 1980. X-ray diffraction study of the insoluble organic matrix of mollusk shells. *FEBS Letters*, **111**, 311–316.

—— —— 1981. Organic matrix–mineral relationships in mollusk shell nacreous layers. 467–482. *In* BALABAN, M., SUSSMAN, J. L., TRAUB, W. and YONATH, A. (eds). *Structural aspects of recognition and assembly in biological macromolecules*. Balaban International Science Services, Rehovot & Philadelphia, 961 pp.

YOUNG, G. A. and NOBLE, J. P. A. 1987. The Llandovery–Wenlock Syringoporidae from New Brunswick, Canada. *Journal of Paleontology*, **61**, 268–283.